AN EXPERIMENTAL INVESTIGATION OF IMPROVED RECOVERY IN FRACTURED CARBONATE SAMPLES FOLLOWING FOAM FLOODING

A Thesis

by

YOSSRA OSMAN

Submitted to the Office of Graduate and Professional Studies of
Texas A&M University
in partial fulfillment of the requirements for the degree of

MASTER OF SCIENCE

Chair of Committee,	Ahmed Abdel-Wahab
Co-Chair of Committee,	Aziz Rahman
Member,	Thomas Seers
Head of Department,	M. Nazmul Karim

May 2019

Major Subject: Chemical Engineering

Copyright 2019 Yossra Osman

ABSTRACT

Due to complex depositional textures and diagenetic processes, carbonate reservoirs are challenging in terms of recovery. This thesis will present the use of foam flooding as a tertiary recovery technique, and as a means of overcoming limitations of pre-existing methods. Two cases were studied in this thesis - Case 1 will present the EOR impact of surfactant flooding on non-fractured carbonate rocks, and Case 2 will present the EOR impact of foam flooding on fractured carbonate rocks. The three core samples used in this study are Indiana limestone carbonate rocks. The cores have an approximate dimension of 13 cm length and 3.8 cm diameter. The porosity is in the range of 13-21% and the permeability is in the of 0.69 -2.17 mD.

In the first case (Case 1), surfactant flooding aims to improve recovery by decreasing the oil-water interfacial tension, thus improving the displacement efficiency. In the second case (Case 2), foam aims to improve recovery by both decreasing the oil-water interfacial tension, and plugging high permeability channels, thus forcing brine to sweep areas of lower permeability.

Prior to implementing any recovery techniques in Case 1 or Case 2, petrophysical properties including porosity, permeability, initial oil saturation and residual water saturation were obtained through mass balance, pressure difference tests during steady state injection and volume balance respectively. For Case 1, recoveries due to waterflooding were in the range of 22.-34 %. For Case 2, waterflooding performed poorer with recoveries in the range of 20 - 27 %. Tertiary recovery (surfactant flooding for Case 1 and foam flooding for Case 2) shows an enhancement in recovery in the range of 0.5 – 5(% of OIP) for Case 1, and 5- 8 (% of OIP) for Case 2. These results prove to be effective for the low surfactant concentration used (0.1%). Low concentration foams and surfactant seem to be a more reasonable choice for the cost-cutting industry of today.

DEDICATION

This thesis is dedicated to my mother and father who have consistently supported me throughout my entire life. I would also like to dedicate it to my brother and sister who have always been there to put a smile on my face. Their unconditional love, support and encouragement is a huge motivation behind my successes.

ACKNOWLEDGEMENTS

I would like to sincerely thank all the members of my committee. A huge thank you to *Dr. Thomas Seers* (supervisor), *Dr. Aziz Rahman* (supervisor) and *Dr. Ahmed Abdel-Wahab* for all their guidance and support throughout the entire course of this research.

I would also like to greatly thank my lab instructor, *Mr. Ibrahim Al-Maghrabi*, for sharing his lab expertise and assisting me throughout this entire project.

A huge thank you goes to *Texas A&M University*, *research faculty*, *start-up grant* and *Qatar Foundati*on for this opportunity and memorable experience.

I would also like to thank some members from industry for their professional input. A big thank you to *Mayur Pal* from NOC and *Oussama Gharbi* from TOTAL for their feedback and professional input.

And of course a huge thank you to my mother, father and siblings for their love, support and encouragement. I would like to specifically acknowledge my brother for his tremendous support throughout. Thank you also to my entire circle of friends and loved ones.

And of course, all thanks due to God.

CONTRIBUTORS AND FUNDING SOURCES

This work was supported by a dissertation committee consisting of two main supervisors, Dr. Thomas Seers and Dr. Aziz Rahman, both from the Petroleum Department. Dr. Ahmad Abdel Wahab, was the chair of this project, from the Chemical Department.

The cores used for this study were provided by Professor Aziz Rahman.

The authors are grateful to the Qatar Foundation and Texas A&M University at Qatar for the experimental facility. The authors would like to acknowledge the start-up fund provided by Texas A&M University, Qatar. This publication was made possible by the grant NPRP10-0101-170091 from Qatar National Research Fund (a member of the Qatar Foundation). Statements made herein are solely the responsibility of the authors.

NOMENCLATURE

A_{cs}	Cross-sectional area [cm^2]
D	Core diameter [cm]
L	Length of the core sample [cm]
k	Permeability [mD]
m_{dry}	Mass of dry core sample [g]
$m_{brine\ saturated}$	Mass of core sample after brine saturation [g]
$m_{(brine + oil)\ saturated}$	Mass of core sample after decane oil saturation [g]
$m_{waterflooding}$	Mass of core sample after primary recovery, waterflooding [g]
$m_{surfactant\ flooding}$	Mass of core sample after secondary recovery, surfactant flooding [g]
$m_{f\ dry}$	Mass of fractured dry core sample [g]
$m_{f\ brine\ saturated}$	Mass of fractured core sample after brine saturation [g]
$m_{f\ (brine + oil)\ saturated}$	Mass of fractured core sample after decane oil saturation [g]
$m_{f\ waterflooding}$	Mass of fractured core sample after primary recovery, waterflooding [g]
$m_{f\ foam\ flooding}$	Mass of fractured core sample after secondary recovery, foam flooding [g]
m_{oil}	Mass of the oil within the rock [g]
m_{oil}	Mass of the oil within the rock [g]
m_{brine}	Mass of the brine within the rock [g]
Δm	Difference between core mass between any two consecutive stages [g]
ΔP	Pressure difference across upstream & downstream terminals of core [Psi]
q	Flowrate [cc/min]
R	Recovery

S_o	Initial Oil Saturation
S_{wr}	Irreducible Water Saturation
S_{or}	Irreducible Oil Saturation
S_w	Water Saturation
V_{bulk}	Bulk volume [cc]
V_{pore}	Volume of pores [cc]
V_{brine}	Volume of brine [cc]
$V_{oil\ initial}$	The initial volume of oil inside the core before any recovery [cc]
$V_{oil\ waterflooding}$	The volume of oil inside core following waterflooding recovery [cc]
$V_{oil\ surfactant\ flooding}$	The volume of oil inside core following surfactant flooding recovery [cc]
ΔV_{oil}	Volume of the oil that was expelled [cc]
ρ_{brine}	Density of brine [g/cc]
Φ	Porosity
μ	Viscosity of the brine flooding fluid [cP]

TABLE OF CONTENTS

Page

LIST OF FIGURES

Page

LIST OF TABLES

Page

CHAPTER I

INTRODUCTION AND LITERATURE REVIEW

1.1 Carbonate Reservoirs

With the global increase in the demand for crude oil, the need to develop enhanced oil recovery techniques is crucial. These techniques must focus on how to displace greater volumes of trapped oil from within a given rock [1, 4, 10, 12]. Since carbonate reservoirs constitute of over half of the world's oil reserves, research has recently shifted its focus on recovery techniques as they pertain to carbonate reservoirs [5].

All carbonate rocks are heterogeneous to varying degrees and many carbonate reservoirs are naturally fractured. Due to the lack of homogeneity in carbonate reservoirs, the porous media is naturally composed of a variety of pore sizes, pore throats, vugs and fractures [3]. This can often be a cause of non-uniform displacement, making carbonate reservoirs inherently more challenging in terms of recovery [5]. As a result, carbonate reservoirs continue to face complications with pre-existing IOR techniques, such as waterflooding and gas flooding.

1.2 Complications of Pre-existing Recovery Techniques

Previous research has been conducted to investigate the results of primary, secondary and tertiary recovery techniques on carbonate reservoirs. Primary recovery techniques alone have shown to yield a recovery of less than 10% of the original oil in place (OOIP) [13]. An improvement is seen with waterflooding, a common and economic secondary recovery technique [8, 9], however, the recovery is still not optimized with waterflooding. The issue with waterflooding in carbonate reservoirs is that water tends to flow through the high permeability channels or fractures, thus leaving large portions of the oil in the reservoir unswept. Consequently,

only a maximum of 35% of the OOIP is swept when implementing secondary recovery waterflooding techniques [13].

Another secondary recovery technique which can be used on carbonate reservoirs is gas flooding. Although gas flooding is another common and economic recovery technique, again it faces major issues in carbonate formations. One of those issues is viscous fingering which results due to a considerably lower viscosity of the injected gas (N_2, CO_2 etc.) in comparison to the oil/brine being swept. This results in gas flowing through the fracture, leaving large portions of the reservoir unswept and significant volumes of the oil left unrecovered.

1.3 Foam Flooding in EOR

Due to the shortcomings of pre-existing primary and secondary recovery techniques in IOR, the need to investigate the future of foam as a territory recovery technique has become more important. To increase oil recovery, one of two strategies must be achieved. The first is to increase the overall volume of oil being swept, and the second is to improve the displacement efficiency [2, 11]. Foam is useful in achieving both and therefore is an efficient recovery technique.

Concerning the first strategy, foam can increase the overall volume of oil being swept by improving the sweep efficiency. This can be explained due to the considerably higher apparent viscosity of foam, in comparison to that of water or gas, which translates into better control of viscous fingering and thus improved sweeping [6]. Foam also improves sweep efficiency by plugging high permeability zones such as pore throats and fractures, and thus forcing the flooding fluid to sweep areas of lower permeability [2, 11]. This is particularly relevant to carbonate formations due to their heterogeneous nature. Foam will block the fracture first, and then divert the flooding fluid (brine) into the lower permeability zones [2, 11, 14]. Concerning the second

strategy, foam can improve the displacement efficiency by decreasing the oil-water interfacial tension. This is because foam is composed of surfactant which is known to decrease oil-water interfacial tension as well as change the rock wettability from oil-wet to water-wet, making it easier to extract the oil [6, 13]. It is clear that it is a particularly useful resource which can be utilized to tackle the difficulties in carbonate formations and improve oil recovery.

Literature has shown that tertiary recovery using foam and surfactant flooding can yield a recovery of up to 5-10 % of the OOIP [13]. This additional recovery has tremendous value when up-scaled to real life production. **Table 1** below displays a summary of the three recovery techniques discussed above and the recoveries they yield according to the following cited sources.

Table 1. Recovery PercentageS for different Recovery Techniques, Adapted from [13]

Recovery Technique	Recovery of OOIP R %
Primary recovery	10
Secondary recovery (Water/ Gas Flooding)	0-35
Tertiary recovery (Foam/Surfactant Flooding)	5-10

CHAPTER II

MATERIALS

2.1 Raw Materials

2.1.1 Surfactant

The surfactant *Platinum Foam Plus* used in this study is a commonly used drilling fluid additive. It was supplied by MI SWACO, Houston Texas. In this paper, we investigate its use as an EOR product due to its ability to reduce the interfacial tension and alter the rock wettability. The changes in these properties were not measured in this investigation, but the effects of them were evident by the improvement in recovery. The physical and chemical properties of Platinum Foam Plus are summarized below in **Table 2**.

Table 2. Physical and Chemical Properties of Platinum Foam Plus

Property	Description
Color	Clear
Odor	Mild Polyether
Physical State	Liquid
pH	6.5 - 8.5 @ 10% Aqueous Solution
Specific gravity (H_2O = 1)	1.04
Solubility (Water)	Soluble
Flash Point: F (^{0}C)	142 F (61.1 C)

2.1.2 Porous Media

The core samples used in this study are Indiana Limestone packstone carbonate rocks. The samples were ordered from the USA. **Figure 1** below displays a thin section of the porous media which was used in this study. Marked on the figure are some interesting features of the core. The thin section shows some shell fragmentation and calcite cementation, with disconnected pore spaces. Other interesting geological features can also be observed such as the Echinoderm spine.

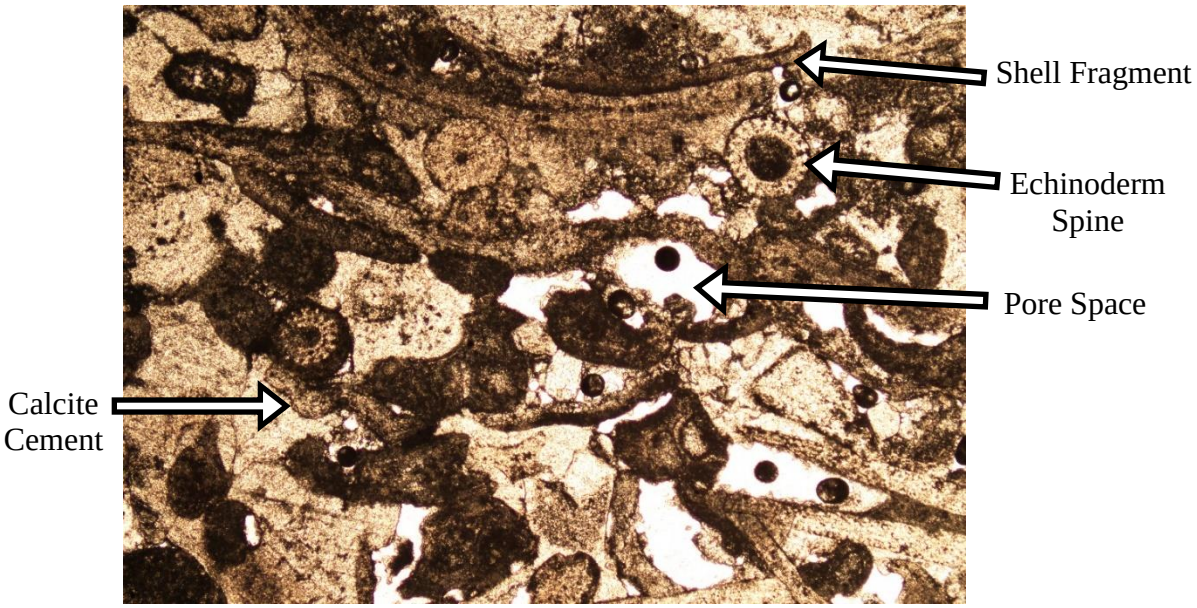

Figure 1. Porous Media Thin Section Image

The three core samples used in this study are named FD3H, FD4H and FD5C. The properties and dimensions of the cores are summarized below in **Table 3**. For a comprehensive discussion on the methods used to calculate the values below, refer to Chapter III, *Setup and Experimental Procedure* and Chapter IV, *Theory*.

Table 3. Dimensions and Properties of Core Samples

Core Sample	Length L	Diameter D	Cross Section Area A_{cs}	Bulk Volume V_{bulk}	Volume of Pores V_{pore}	Dry Mass m_{dry}	Porosity Φ	Permeability k
	cm	*cm*	*cm^2*	*cc*	*cc*	*g*	*%*	*mD*
FD3H	12.93	3.78	11.25	145.41	18.83	329.38	13	2.17
FD4H	13.09	3.78	11.22	146.87	19	334.25	13	1.80
FD5C	12.98	3.77	11.14	144.7	30.04	300.27	21	0.69

2.1.3 Oil

The oil used in this study was n-Decane ($C_{10}H_{22}$). It has a molecular weight of 142.28 g/ mole and a density of 0.73 g/cc at T = 20 º C.

2.2 Prepared Materials

2.2.1 Preparation of Surfactant Solution

The surfactant fluid was prepared in the laboratory at ambient room temperature in a ratio of 1000 milliliters of water to 1 milliliter of liquid surfactant, yielding an overall concentration of 0.1 vol. %. Water was used as the diluting agent and a magnetic mixing machine was used to mix the components. Surfactant concentration was not a sensitivity parameter in this investigation, so a single concentration value of 0.1 vol. % was used for this entire investigation. It is clear that an increase in surfactant concentration would also yield to an increase in recovery, however also an increase in cost. Therefore, a low surfactant concertation value was selected in aim to investigate a cost-effective EOR technique. In the future, it may be beneficial to perform a cost analysis test to determine the optimum balance between surfactant concentration, cost and profitability

2.2.2 Preparation of Brine Solution

Standard sodium chloride (NaCl) was used for preparation of the brine solution. The brine solution was prepared at ambient room temperature in a ratio of 1000 g of water to 20 g of NaCl, yielding an overall concentration of 2 wt. %. The components were mixed manually using a stirring rod. The choice of brine concentration was based off of typical values used for experimental work. This salinity is not too far from the salinity observed in the gulf region. For the purpose of simplicity, the same brine solution was used for core saturation and waterflooding recovery.

2.3 Apparatus

2.3.1 Core Flow Loop

The core flow loop is shown below in **Figure 2**:

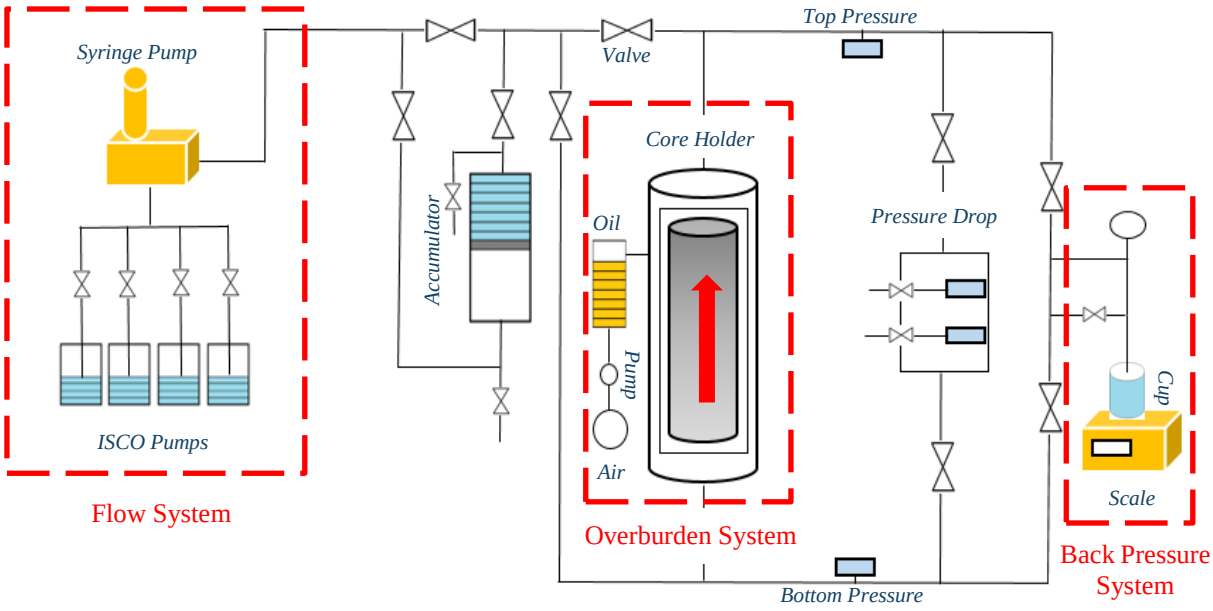

Figure 2. Core Flow Loop Schematic

The core flow loop shown above is the shorter loop which does not include the foam loop. This experimental set-up was used for permeability measurements, oil saturation, waterflooding

and surfactant flooding. The core flow loop is composed of three main systems which have been highlighted in red in the above figure. Those are:

i. The flow system,
ii. The overburden system
iii. The back-pressure system

The flow system, shown to the left of the schematic, is mainly operated through a set of pumps. The syringe pump, composed of a set of ISCO pumps, is in charge of generating the flow of fluid into the core.

The overburden system, shown in the center of the schematic, is the system which generates pressure around the core. This pressure is generated by injecting pressurizing liquid oil into the annular volume which forms between the inside of the core holder and the outside of the core sleeve. This pressurized liquid exerts a pressure on the core sleeve, which in turn exerts a pressure on the core, creating what is known as the overburden pressure. The overburden pressure ensures that the core sample stays in place during the test, the flow is linear across the core sample and that the sleeve does not break loose as pressurized fluids are injected. This overburden pressure must always be set 150 psi greater than the inlet pressure of the core holder. It should be increased gradually and in accordance to the inlet pressure to ensure that a 150 psi difference maintained. Increasing the overburden pressure too quickly/too much can cause the core to break/fracture.

Finally, the back pressure system, to the right of the schematic, controls the outlet pressure during core flow. A back pressure system is installed at the core outlet to ensure that the fluids do not return back at a dangerously high velocity due to large pressure gradients. Hence, the backpressure system reduces the very high outlet pressure such that the fluids exiting the core can safely be collected. Fluid contents in the container may be useful when one is examining recovery.

2.3.2 Combined Flow Loop

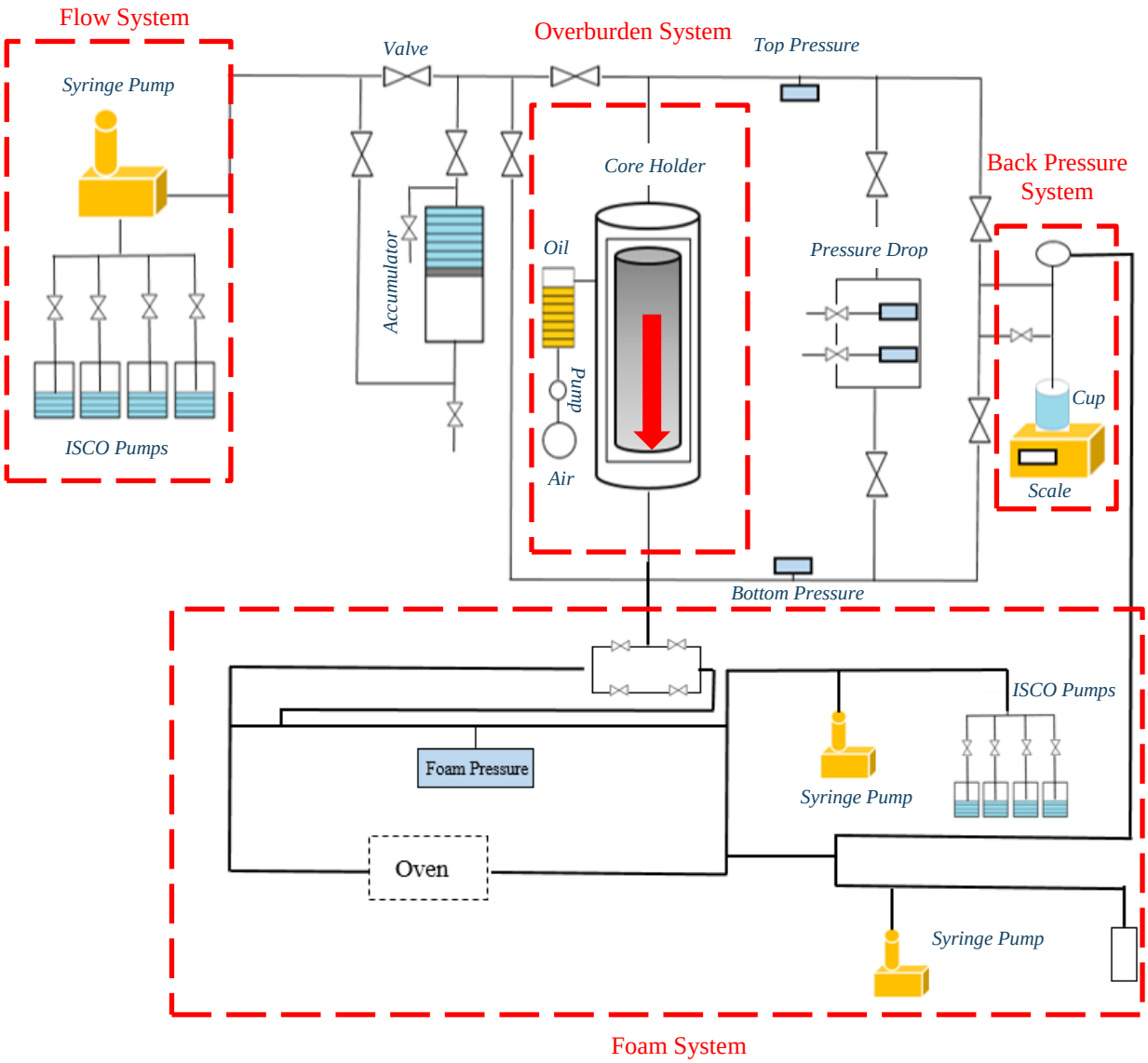

Figure 3. Combined Flow Loop Schematic

The combined flow loop (**Figure 3**) shown above is the longer loop which includes the core flow loop plus the foam loop. This experimental set-up was only used for foam flooding. The combined flow loop is now composed of four main systems which have been highlighted in red in the above figure. Those are:

i. The flow system,
ii. The overburden system
iii. The back-pressure system
iv. The foam system

The core flow loop remains exactly the same as what was discussed above. This time however, an additional foam loop system is connected to the core flow system via a ¼" tubing which attaches at the inlet of the core holder. The foam loop is in charge of generating foam by mixing surfactant solution with Nitrogen gas. Once foam is generated it enters the core flow loop for regular flooding.

CHAPTER III

SETUP AND EXPERIMENTAL PROCEDURE

3.1 Case 1: Non- fractured Carbonate Samples

Three carbonate core samples of similar lithology were collected from natural outcrops. The cores had a diameter of around 3.8 cm and a length of around 13 cm. The three samples were named FD3H, FD4H and FD5C and will be referred to as such in the following text. A schematic of the three cores is displayed below in **Figure 4**.

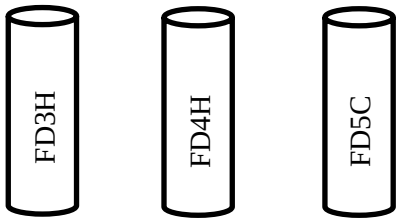

Figure 4. Three Non-fractured Carbonate Core Samples

3.1.1 Core Measurements

Core dimensions were taken using a digital caliper. Dimensions noted were diameter and Length. Three measurements were taken, and an average was found for reliability.

3.1.2 Porosity Measurement

Porosity measurements were carried out using two experimental methods. The first experimental method applied was Archimedes' classical method of weights, and the second experimental method applied was based on thin section analysis. Both methods will be discussed below.

3.1.2.1 Experimental Method 1 (Archimedes Method)

To begin, the dry mass of each core sample was measured on an electronic scale prior to saturation. In order to ensure that the rocks were completely dry, they were placed inside a lab oven (T = 50 ° C) for 24 hours to evaporate any remaining trapped liquid. Dry masses were recorded for FD3H, FD4H and FD5C.

Next, a 2 wt. % brine solution was prepared using water and Sodium Chloride (NaCl) in the ratio of 1000 ml of water to 20 g of salt. The core samples were then placed inside a vacuumed cell for 8 to 10 hours. After this duration passed, the vessel was filled with 2 wt. % brine solution such that the core samples were fully submerged. The samples were left inside the locked saturation vessel for three days (72 hours). The tightly pressurized vessel is designed to facilitate the saturation of fluid within the core. Following this duration, the vessel was de-pressurized and the samples were removed. Although 100% saturation cannot be guaranteed, this method is still fairly efficient. The same electronic scale that was used to record dry mass was used to record the saturated mass of each of the three core samples to ensure consistency. Based on the dry and saturated mass of each sample, the porosity was calculated for each core using Archimedes method. Following the saturation procedure, the samples were then stored within a small plastic container filled with the brine to ensure that the samples remain saturated until the next flooding experiment.

3.1.2.2 Experimental Method 2 (Thin Section Analysis)

The porosity values were verified using a second method: thin section analysis. This method was only applied to one of the rock samples, FD3H once all the experimental work was complete for both Case 1 and Case 2. The core of interest, FD3H, was cleaned and dried to return it to its original state. This procedure was done in a soxhlet extractor. The cores were cleaned using

dean-stark apparatus with hot toluene followed by methanol. Toluene was used to strip any oil traces inside the core and methanol was used to remove any salt. The cores were then placed in the lab oven (50^{o}C) to dry overnight.

In order to obtain a thin section, the core was cut into a mineral chip and then it was grinded down to a a thickness of 30 microns. The thin section was approximately 25 mm by 25 mm.

After the thin sections were ready, they were placed under a polarizing microscope. The eye lens magnification was constant (x10) and the object length magnification was varied until a good focus was obtained. The total magnification was given by the eye lens magnification multiplies by the object length magnification. The images were captured using the software (NIS) element BR. A MATLAB program was designed to estimate the porosity from the image. The program's tracing tool was used to trace the pore area, by drawing several polygons to cover the entire pore space. The program then estimated this area relative to the area of the full image and outputted a percentage porosity. This process was repeated twice on different areas of the thin section and an average was taken to increase reliability.

3.1.3 Permeability Measurements

After porosity measurements were taken, permeability measurements were conducted in the core flooding unit. Each core was placed inside the core holder and secured for each independent test. The accumulator was filled with brine solution. A top flush and a bottom flush were conducted to purge the lines and remove any trapped air from the system.

The core was inserted into the core holder, and the overburden pressure was initially set at an arbitrary value. The following value does not have a particular specification, however, it should always be set 150 psi greater than the pressure drop across the core. The overburden pressure was not set too high since it could alter the rock structure and permeability. In this

particular case the overburden pressure was initially set at 600 psi, knowing that the pressure drop across the core sample will not exceed 450 psi at the beginning of core flooding. As the test proceeded, the pressure difference across the core was monitored, and whenever this pressure drop value came close to exceeding the overburden pressure, the overburden pressure was adjusted accordingly. All tests were conducted under pressurized conditions similar to reservoir conditions, but not specific to a particular reservoir. The tests were not conducted under reservoir temperature.

Once the overburden pressure was adjusted, an initial flowrate of 0.5 cc/min (2 wt. % brine) was set. During flooding, a real time data log of pressure drop across the core (ΔP) vs. flowrate (Q) was recorded. Once ΔP stabilized, it was recorded and the flowrate was increased again by 0.2 cc/min. This process was conducted for three flowrates: 0.5 cc/min, 0.7 cc/min and 0.9 cc/min. Once a stabilized value of ΔP was attained and recorded for each flowrate, a plot of ΔP vs. Q was created. From this plot, permeability was calculated using Darcy's Equation.

The samples were removed from the core holder and then stored within a small plastic container filled with 2 wt. % brine to ensure that the samples remained saturated until the next flooding experiment.

3.1.4 Oil Saturation

After permeability tests were complete, the core samples containing brine, were ready for decane saturation.

This procedure was conducted inside the same flooding unit. The accumulator was emptied, cleaned and filled with sufficient decane. Again, a top flush and a bottom flush were conducted to purge the lines and remove any trapped air from the system. The core was placed and secured inside the core holder with the overburden pressure set and monitored in the same way as is described in the permeability section above.

Decane was injected at 2 cc/min for around 5 to 6 pore volumes to ensure that the irreducible water saturation ($\mathbf{S_{wr}}$) was reached, and hence the correct initial oil saturation (S_o).

Following decane injection, each sample was weighed and stored within a small plastic container filled with decane to ensure that they remain saturated until the next flooding experiment.

3.1.5 Waterflooding: Secondary Recovery

After decane saturation, the core samples containing brine and decane were ready for recovery, starting with waterflooding.

The accumulator was emptied, cleaned and re-filled with brine. Again, a top flush and a bottom flush were conducted to purge the lines and remove any trapped air from the system. The core sample was then inserted into the core holder and the overburden pressure was set and monitored in the same way as is described in the permeability section above.

Brine was injected at a flowrate of 1 cc/min for around 6 to 7 pore volumes to ensure that the residual oil saturation ($\mathbf{S_{or}}$) was achieved. A beaker was placed at the outlet of the flooding apparatus to collect the fluid exiting the core sample. The pressure drop across the sample was monitored and plotted as a function of time and number of pore volumes injected. The point at which the first drop of water was observed was identified as the water breakthrough point.

After the test was complete, the samples were weighed on the same electronic scale and then stored within a small plastic container filled with decane to ensure they remain saturated until the next flooding experiment.

3.1.6 Surfactant flooding: Tertiary Recovery

Following waterflooding, the cores (still containing brine and decane) were ready for tertiary recovery (surfactant flooding).

First, the surfactant mixture was prepared in the ratio of 1000 milliliters of water to 1 milliliter of liquid surfactant. The components were mixed together using a magnetic stirrer, yielding an overall concentration of 0.10 vol. % to 2 decimal places.

The accumulator was emptied, cleaned and re-filled with the surfactant solution. Again, a top flush and a bottom flush were conducted to purge the lines and remove any trapped air from the system. The core sample was then inserted into the core holder and the overburden pressure was set and monitored as before.

Surfactant was injected at a flowrate of around 1 cc/min for around 7 to 8 pore volumes to ensure that irreducible oil saturation (S_{or}) was achieved. A beaker was placed at the outlet of the flooding apparatus to collect the fluid exiting the core sample. The pressure drop across the sample was monitored and plotted as a function of time and number of pore volumes injected. The point at which the first drop of surfactant was observed was identified as the surfactant breakthrough point.

After the test was completed, the samples were weighed on the same electronic scale.

Figure 5 below shows a summary of the experimental procedure for Case 1.

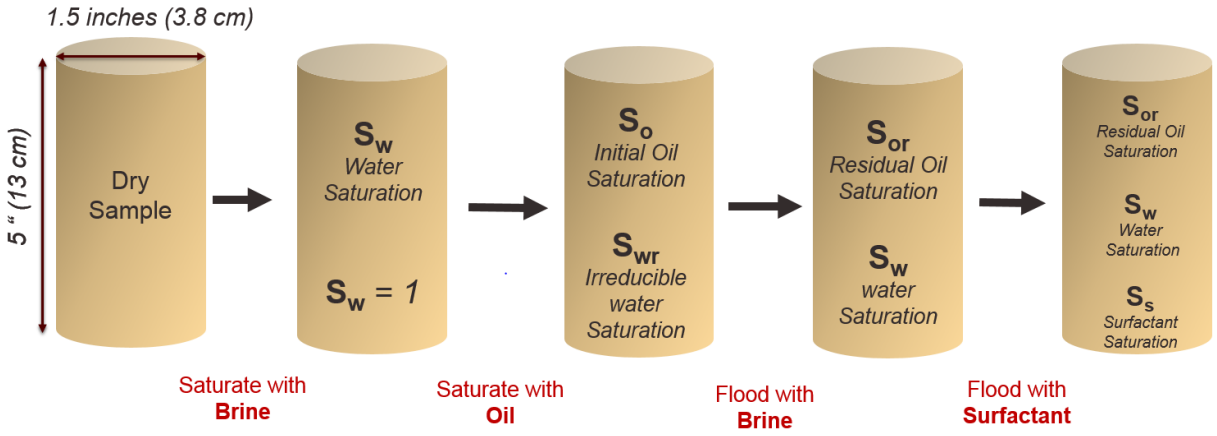

Figure 5. Summarized Experimental Procedure for Case 1

3.2 Case 2: Fractured Carbonate Samples

In Case 2, almost the same experimental procedure was repeated, this time for fractured carbonate samples. Two of the three carbonate samples used in Case 1, FD3H and FD4H, were re-used for this experiment. The samples went through a stringent cleaning and drying process to return them to their original state. Additionally, the samples were fractured to represent fractured carbonate lithology for the purpose of the study in Case 2. The dimensions of the core remained roughly the same as in Case 1. **Figure 6** below displays a schematic of the two fractured core samples used in Case 2.

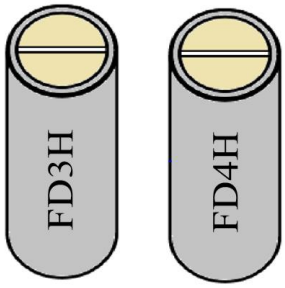

Figure 6. Two Fractured Carbonate Core Samples used in Case 2

It is important to note that the core was first saturated with brine and then decane before it was fractured. This is because attempting to saturate the cores with brine and decane after fracturing would mean that the cores would have been partially saturated (as fluid would have bypassed the fracture). The below discussion will represent the procedure for Case 2 sequentially.

3.2.1 Brine Saturation

First, the two samples were re-saturated with 2 wt. % brine using the same saturation vessel. The exact same procedure as in Case 1 was repeated. Please refer to Case 1 for more details.

3.2.2 Oil Flooding

Following brine saturation, the two samples were saturated with n-decane using the same flooding apparatus. The exact same procedure as in Case 1 was repeated. Please refer to Case 1 for more details.

3.2.3 Creating the Fracture

Following brine and decane saturation, the cores were fully saturated and ready for fracturing. A vertical fracture, perpendicular to the cross-section of the core, was created across the length of the core using a saw cutting machine. To hold the two almost symmetrical halves together, while keeping the fracture slightly open, a couple of steps were taken:

i. A permeable filling was created to keep the fracture somewhat open
ii. Tin foil was wrapped around the circumferential area of the core to hold it together (Foil jacketing), whilst leaving the inlet and outlet ends uncovered

The filling consisted of filter paper folded and compacted together to forms a slim, porous and permeable rectangular prism with a length and width equal to that of the core length and diameter respectively and a height of around 0.2 cm. **Figure 7** below displays a schematic of a fractured core sample and the fracture filling which keeps the fracture open.

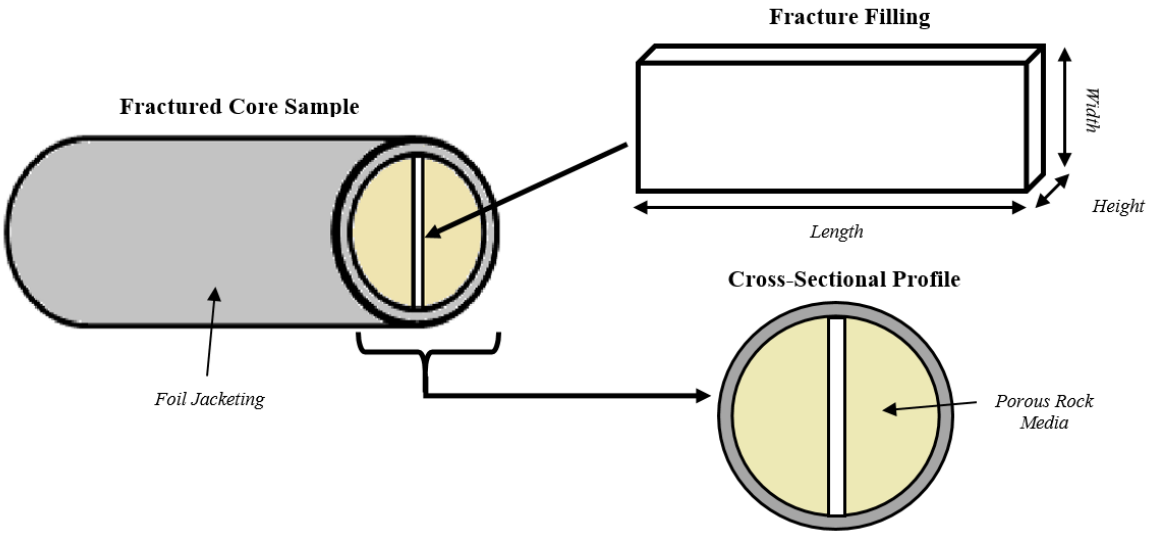

Figure 7. Schematic of Fractured Core Sample and the Fracture Filling

Once each fractured core was prepared, as per the above schematic, the decane saturated fractured core mass was recorded. The samples were stored within a small plastic container filled with decane to ensure they remain saturated until the next flooding experiment.

3.2.4 Waterflooding: Secondary Recovery

After the samples were prepared, the fractured core samples containing brine and decane were ready for recovery. The first recovery method implemented was waterflooding. The exact same procedure was conducted as before (refer to Case 1 for more detail). Extra caution was taken in placing the core sample inside the core holder since the core was only held together by tin foil jacketing. During testing, the overburden pressure applied on the core held it together tightly.

Once the test was complete, each core sample was removed and weighed. This weight represented the fractured core weight after waterflooding, which includes the weight of the foil jacketing, fracture filling and rock.

3.2.5 Foam flooding: Tertiary Recovery

Following waterflooding, the samples still containing brine and decane were ready for tertiary recovery (foam flooding). The properties of foam make it specifically beneficial for the investigation of Case 2. This time surfactant was prepared as a two phase mixture with nitrogen gas in order to form 'foam'. The general term 'foam flooding' will be used in this text to describe a sequence of two injections: a short foam flooding injection followed by a waterflooding injection (in which brine acts as the sweeping agent).

Whereas in Case 1 the core flow loop apparatus was used alone, in Case 2 the 'core flow loop' (**Figure 2**) was combined with the 'foam loop' to form the 'Combined Flow Loop' (**Figure 3**). In order to connect the 'foam loop' to the 'core flow loop', a ¼" tubing was connected from the inlet of the core holder to the foam loop section. This can be seen in **Figure 3**.

Next, the two solutions required for this experiment, surfactant 0.1 vol. % (used to generate foam) and 2 wt. % brine (sweeping fluid after foam injection) were prepared in the same ratio.

The 'core loop accumulator', and 'foam loop' accumulator were then cleaned, emptied and re-filled with brine solution and surfactant solution respectively. Again, a top flush and a bottom flush were conducted to purge the lines and remove any trapped air from the system. The core sample was then inserted into the core holder carefully and the overburden pressure was set and monitored as before.

The system was then changed to a 'combined mode' on the software options and the foam was generated in the long loop. Target conditions were set for the foam including properties such as density, temperature and pressure.

Now, the system was ready for foam flooding. Foam was injected upward through the core at around 1-2 cc /min for a short duration (only a few pore volumes).

Once foam was injected for a few pore volumes, the test was ended, and the core sample was removed and weighed using the same electronic scale. This mass included the weight of the rock jacketing, the fracture filling and the rock itself.

After the weight was recorded, the core was carefully re-placed back into the core holder and the system was switched back to 'core flow mode' to conduct brine injection. A beaker was placed at the outlet of the flooding apparatus to collect the fluid exiting the core sample (mostly foam displaced by brine). Brine was injected for around 3-4 pore volumes and then the test was stopped, and the core sample was removed and weighed. Again, this mass included the weight of the rock jacketing, the fracture filling and the rock itself.

3.2.6 Porosity Measurement

Following the full set of flooding experiments, it was necessary to obtain the dry weight and the brine saturated weight of the *fractured sample* in order to calculate the porosity and pore volume. To obtain the dry weight of the fractured cores, the cores were cleaned and dried to return to them to their original condition. This process involved:

i. Flushing the fluids in the core out using water
ii. Evaporating any fluids within the cores by placing samples in an oven

Once this was complete the dry weight including the fracture filling and foil jacketing was taken. The dimensions of the core were also taken to calculate the bulk volume. Next, the cores were placed in a brine saturation vessel in the same way as discussed in Case 1, and the brine saturated weight was taken (including the fracture filling and foil jacketing). Porosity was then calculated using Archimedes method.

Figure 8 below summarizes the experimental procedure for Case 2.

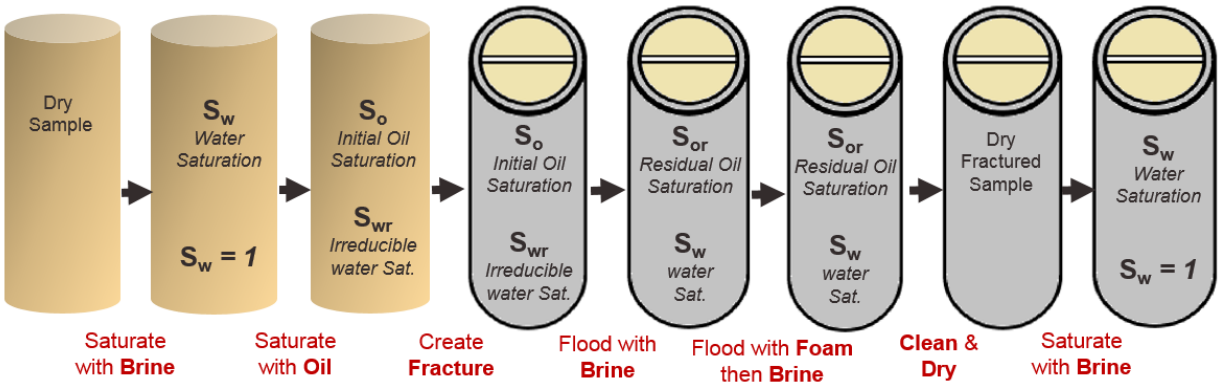

Figure 8. Summarized Experimental Procedure for Case 2

CHAPTER IV

THEORY

4.1 Case 1: Non- fractured Carbonate Samples

For the theory section the following parameters need to be defined. These parameters will define the mass of the core throughout the transitional stages of the experimental procedure of Case 1. There are five stages at which the mass was recorded. These stages are summarized in the **Table 4** below.

Table 4. Mass of the Core at Different Stages of the Experiment for Case 1

Stage	Nomenclature	Mass	Core Sample Contents
1	m_{dry}	Dry core sample	NA
2	$m_{brine\ saturated}$	Core sample after brine saturation	Brine
3	$m_{(brine + oil)\ saturated}$	Core sample after decane oil saturation	Brine n-Decane
4	$m_{waterflooding}$	Core sample after primary recovery, waterflooding	Brine n-Decane
5	$m_{surfactant\ flooding}$	Core sample after secondary recovery, surfactant flooding	Brine n-Decane Surfactant

4.1.1 Porosity Calculations

In this section, the porosity calculations based on Archimedes method will be discussed. Porosity is defined as the ratio of pore volume to bulk volume. Therefore, both the pore volume and the bulk volume must be obtained. Bulk volume ($\mathbf{V_{bulk}}$) is defined as the product of the cross-sectional area ($\mathbf{A_{cs}}$) by the core length (**L**).

Let:

V_{bulk} : Bulk volume (cc)

A_{cs} : Cross-sectional area (cm^2)

L : Core length (cm)

D : Core diameter (cm)

Equation 1

$$V_{bulk} = A_{cs}L \quad \rightarrow \quad V_{bulk} = \left(\frac{\pi d^2}{4}\right)L$$

After the bulk volume for both samples were calculated, the difference, delta mass (**Δm**), between the brine saturated core mass (**$m_{brine\ saturated}$**) and the dry core mass (**m_{dry}**) was calculated.

Let:

Δ m : Difference between brine saturated core mass and the dry core mass (g)

Equation 2

$$\Delta m = m_{\text{brine saturated}} - m_{dry}$$

This difference in mass (**Δm**) represents the mass of the brine within the rock sample. When this mass is divided by the density of brine (**ρ_{brine}**) the volume of brine (**V_{brine}**) is obtained. If the core is fully saturated, we can assume that volume of brine is equal to the pore volume (**V_{pore}**).

Let:

ρ_{brine} : Density of brine (g/cc)

V_{brine} : Volume of brine (cc)

V_{pore} : Volume of pores (cc)

Equation 3

$$\therefore V_{pore} = V_{brine} = \frac{\Delta m}{\rho_{brine}}$$

Dividing the pore volume by the bulk volume, the porosity of the core is obtained.

Let:

Φ : Porosity

Equation 4

$$\therefore \ \Phi = \frac{V_{pore}}{V_{bulk}}$$

4.1.2 Permeability Calculations

Permeability calculations were conducted through the flooding procedures explained above in Chapter III: Setup and Experimental Procedure. All calculations were conducted based on Darcy's Law as shown in **Equation 5**.

Let:

Q : Flowrate (cm^3/s)

k : Permeability (D)

A_{cs} : Cross-sectional area of the core (cm^2)

μ : Viscosity of the brine flooding fluid (cP)

L : Length of the core sample (cm)

ΔP : Pressure difference across the upstream & downstream terminals of core (atm)

Equation 5

$$\boldsymbol{Q = \frac{kA_{cs}}{u\,L}\,(\Delta p)}$$

Plotting **ΔP** vs. **Q,** a linear graph is obtained where ΔP represents y, Q represents x, and ($\frac{u\,L}{k\,A_{cs}}$) represents the slope, m. Therefore, if we re-arrange Equation 5 above into the form of the straight line equation we obtain:

Equation 6

$$\Delta p = \left(\frac{u\,L}{k\,A_{cs}} \right) Q \rightarrow y = mx + c$$

Equation 7

$$\therefore slope = \frac{u\,L}{k\,A_{cs}}$$

Therefore, the permeability, in Darcys, can be defined as:

Equation 8

$$k = \frac{\mu\,L}{(slope)A_{cs}}$$

4.1.3 Saturation Calculations

The initial oil saturation (**S_o**) and the irreducible water saturation (**S_{wr}**) were calculated after the brine saturated core was flooded with decane. Following oil flooding, Stage 3 in **Table 4,** the core now containing decane and brine was weighed, Stage 3 in **Table 4**. The core sample mass after oil flooding, given by (**$m_{(brine + oil) saturated}$**), was used to calculate the volume of oil (**V_{oil}**) and the volume of brine (**V_{brine}**) through material balance.

The total core mass at stage 3 (**$m_{(brine + oil) saturated}$**) is a sum of the dry core mass, the mass of the oil inside and the mass of the brine inside.

Let:

m_{oil} : Mass of the oil within the rock (g)

m_{brine} : Mass of the brine within the rock (g)

Therefore, the total mass of the core at the end of stage 3 is given by **Equation 9**.

Equation 9

$$m_{\,(brine+oil)\,saturated} = m_{dry\,core} + m_{\,oil} + m_{\,brine}$$

Where the density is expressed as the ratio of mass over volume. Re-arranging, the mass can be expressed as the product of density and volume.

Equation 10

$$\rho = \frac{m}{V} \qquad \rightarrow \qquad m = \rho V$$

Substituting **Equation 10** in **Equation 9** we get **Equation 11**:

Equation 11

$$m_{\,(brine+oil)\,saturated} = m_{dry\,core} + (\rho_{\,oil} V_{\,oil}) + (\rho_{\,brine} V_{\,brine})$$

Since the pore volume contains both brine and decane, the volume of brine within the pores (**V_{brine}**) can be expressed as the pore volume (**V_{pore}**) minus the volume of oil (**V_{oil}**).

Equation 12

$$V_{brine} = V_{pore} - V_{oil}$$

Substituting **Equation 12** in **Equation 11** we get **Equation 13**:

Equation 13

$$m_{\,(brine+oil)\,saturated} = m_{dry\,core} + \rho_{\,oil} V_{\,oil} + \rho_{\,brine}\,(V_{\,pore} - V_{oil})$$

Multiplying out the brackets we get **Equation 14**:

Equation 14

$$m_{\,(brine+oil)\,saturated} = m_{dry\,core} + \rho_{\,oil} V_{\,oil} + \rho_{\,brine} V_{\,pore} - \rho_{\,brine} V_{oil}$$

Re-arranging **Equation 14** and solving for the volume of oil (**V_{Oil}**) we get **Equation 15**

$$V_{oil}(\rho_{oil} - \rho_{brine}) = m_{(brine+oil)\,saturated} - m_{dry\,core} - \rho_{brine} V_{pore}$$

Equation 15

$$V_{oil} = \frac{(m_{(brine+oil)\,saturated} - m_{dry\,core} - \rho_{brine} V_{pore})}{(\rho_{oil} - \rho_{brine})}$$

And the volume of brine (**V_{brine}**) can be expressed as shown in **Equation 16**:

Equation 16

$$V_{brine} = V_{pore} - \frac{(m_{(brine+oil)\,saturated} - m_{dry\,core} - \rho_{brine} V_{pore})}{(\rho_{oil} - \rho_{brine})})$$

Now, the initial oil saturation and the irreducible water saturation can be calculated.

Let:

S_o : Initial Oil Saturation

S_{wr} : Irreducible Water Saturation

The initial oil saturation (**S_o**) is given by **Equation 17**:

Equation 17

$$S_o = \frac{V_{oil}}{V_{pore}}$$

The irreducible water saturation (**S_{wr}**) is given by **Equation 18**:

Equation 18

$$S_{wr} = \frac{V_{brine}}{V_{pore}} = 1 - S_o$$

4.1.4 Secondary Recovery Calculation: Waterflooding

Following brine saturation and decane saturation the rock was now ready for secondary recovery: waterflooding. Calculations were done after waterflooding to calculate the residual oil saturation (**S_{or}**), the water saturation (**S_w**), and the recovery (**R**). Following waterflooding, Stage 4 in **Table 4**, the core, still containing oil and brine, was weighed. The core sample mass after waterflooding is given by (**$m_{waterflooding}$**). Again, material balance calculations were re-applied to determine the new volume of oil (**V_{oil}**) and brine (**V_{brine}**) to determine the recovery following waterflooding.

The total core mass at stage 4 (**$m_{waterflooding}$**) is a sum of the dry core mass, the mass of the oil inside and the mass of the brine inside. Therefore, the total mass of the core at the end of stage 4 is given by **Equation 19**.

Equation 19

$$m_{waterflooding} = m_{dry\ core} + m_{oil} + m_{brine}$$

Where the density is expressed as the ratio of mass over volume. Re-arranging, the mass can be expressed as the product of density and volume.

Equation 20

$$\rho = \frac{m}{V} \quad \rightarrow \quad m = \rho V$$

Substituting **Equation 20** in **Equation 19** we get **Equation 21**:

Equation 21

$$m_{waterflooding} = m_{dry\ core} + (\rho_{oil} V_{oil}) + (\rho_{brine} V_{brine})$$

Since the pore volume contains both brine and decane, the volume of brine within the pores (**V_{brine}**) can be expressed as the pore volume (**V_{pore}**) minus the volume of oil (**V_{oil}**).

Equation 22

$$V_{brine} = V_{pore} - V_{oil}$$

Substituting **Equation 22** in **Equation 21** we get **Equation 23**:

Equation 23

$$m_{\,waterflooding} = m_{dry\,core} + \rho_{\,oil} V_{\,oil} + \rho_{\,brine}\,(V_{\,pore} - V_{oil}\,)$$

Multiplying out the brackets we get **Equation 24**:

Equation 24

$$m_{\,waterflooding} = m_{dry\,core} + \rho_{\,oil} V_{\,oil} + \rho_{\,brine}\, V_{\,pore} - \rho_{\,brine}\, V_{oil}$$

Re-arranging **Equation 24** and solving for the volume of oil (**V_{Oil}**) we get **Equation 25**

$$V_{\,oil}(\,\rho_{\,oil} - \rho_{\,brine}\,) = m_{\,waterflooding} - m_{\,dry\,core} - \rho_{\,brine}\, V_{\,pore}$$

Equation 25

$$V_{\,oil} = \frac{(m_{\,waterflooding} - m_{dry\,core} - \rho_{\,brine}\, V_{\,pore})}{(\,\rho_{\,oil} - \rho_{\,brine}\,)}$$

And the volume of brine (**V_{brine}**) can be expressed as shown in **Equation 26**:

Equation 26

$$V_{\,brine} = V_{pore} - \frac{(m_{\,waterflooding} - m_{dry\,core} - \rho_{\,brine}\, V_{\,pore})}{(\,\rho_{\,oil} - \rho_{\,brine}\,)}\,)$$

Now, the residual oil saturation, the water saturation and the recovery can be calculated.

Let:

S_{or} : Residual Oil Saturation

S_{w} : Water Saturation

The residual oil saturation (**S_{or}**) is given by **Equation 27***:*

Equation 27

$$S_o = \frac{V_{oil}}{V_{pore}}$$

The water saturation (**S_{w}**) is given by **Equation 28**:

Equation 28

$$S_w = \frac{V_{brine}}{V_{pore}} = 1 - S_o$$

Next the recovery must be calculated. To calculate recovery, the volume of oil expelled from the rock (**ΔV_{oil}**) is first found by subtracting the volume of oil inside the core after waterflooding (**$V_{oil\ waterflooding}$**) from the initial oil volume (**$V_{oil\ initial}$**) of the core. ΔV_{oil} is given by **Equation 29**.

Let:

ΔV_{oil} : Volume of the oil that was expelled (cc)

$V_{oil\ initial}$: The initial volume of oil inside the core before any recovery (cc)

$V_{oil\ waterflooding}$: The volume of oil inside core following waterflooding recovery (cc)

Equation 29

$$\Delta V_{Oil} = V_{oil\ initial} - V_{oil\ waterflooding}$$

Therefore, the recovery (**R**) can be calculated through **Equation 30**:

Equation 30

$$R = \frac{\Delta V_{oil}}{V_{oil\ initial}}$$

For waterflooding, this recovery represents the recovery as a % of the OIP (oil in place) as well as the recovery as a % of the OOIP (original oil in place).

4.1.5 Tertiary Recovery Calculation: Surfactant Flooding

Following brine saturation, decane saturation and secondary recovery (waterflooding), tertiary recovery was carried out. Calculations were done after surfactant flooding to calculate the residual oil saturation (**S_{or}**), the water saturation (**S_{w}**), the surfactant saturation (**S_s**) and the recovery (**R**). Following surfactant flooding, Stage 5 in **Table 4**, the core, containing oil, brine and surfactant, was weighed. The core sample mass after surfactant flooding is given by (**$m_{surfactant\ flooding}$**). Again, material balance calculations were re-applied to determine the new volume of oil (**V_{oil}**) and brine (**V_{brine}**) to see how much more of the oil was recovered following surfactant flooding.

The total core mass at stage 5 (**$m_{surfactant\ flooding}$**) is a sum of the dry core mass, the mass of the oil inside, the mass of the brine inside and the mass of the surfactant solution inside. Therefore, the total mass of the core at the end of stage 5 is given by **Equation 31**.

Equation 31

$$m_{\ surfactant\ flooding} = m_{dry\ core} + m_{\ oil} + m_{\ brine} + m_{\ surfactant}$$

Where the density is expressed as the ratio of mass over volume. Re-arranging, the mass can be expressed as the product of density and volume.

Equation 32

$$\rho = \frac{m}{V} \qquad \rightarrow \quad m = \rho V$$

Substituting **Equation 32** in **Equation 31** we get **Equation 33**:

Equation 33

$$m_{\,surfactant\ flooding} = m_{dry\ core} + (\rho_{\,oil} V_{\,oil}) + (\rho_{\,brine} V_{\,brine}) + (\rho_{\,surfactant} V_{\,surfactant})$$

Since the pore volume contains brine, decane and surfactant, the volume of brine within the pores ($\mathbf{V_{brine}}$) can be expressed as the pore volume ($\mathbf{V_{pore}}$) minus the volume of oil ($\mathbf{V_{oil}}$) and the volume of the surfactant ($\mathbf{V_{surfactant}}$).

Equation 34

$$V_{brine} = V_{pore} - V_{oil} - V_{surfactant}$$

Substituting **Equation 34** in **Equation 33** we get **Equation 35**:

Equation 35

$$m_{\,surfactant\ flooding} = m_{dry\ core} + \rho_{\,oil} V_{\,oil} + \rho_{\,brine} (V_{\,pore} - V_{oil} - V_{surfactant}) + (\rho_{\,surfactant} V_{\,surfactant})$$

Multiplying out the brackets we get **Equation 36**:

Equation 36

$$m_{\,surfactant\ flooding} = m_{dry\ core} + \rho_{\,oil} V_{\,oil} + \rho_{\,brine} V_{\,pore} - \rho_{\,brine} V_{oil} - \rho_{\,brine} V_{surfactant} + \rho_{\,surfactant} V_{surfactant}$$

Re-arranging **Equation 36** and solving for the volume of oil ($\mathbf{V_{oil}}$) we get **Equation 37**

$$V_{oil}(\rho_{oil} - \rho_{brine}) = m_{surfactant\ flooding} - m_{dry\ core} -$$

$$\rho_{brine} V_{pore} + \rho_{brine} V_{surfactant} - \rho_{surfactant} V_{surfactant}$$

Taking ($\mathbf{V_{surfactant}}$) as a common factor we get:

$$V_{oil}(\rho_{oil} - \rho_{brine}) = m_{surfactant\ flooding} - m_{dry\ core} -$$

$$\rho_{brine} V_{pore} + V_{surfactant}(\rho_{brine} - \rho_{surfactant})$$

Since in this case the brine density is equal to the surfactant density, the last term $V_{surfactant}(\rho_{brine} - \rho_{surfactant})$ equals zero and the equation becomes:

Equation 37

$$V_{oil} = \frac{(m_{surfactant\ flooding} - m_{dry\ core} - \rho_{brine} V_{pore})}{(\rho_{oil} - \rho_{brine})}$$

And the volume of brine ($\mathbf{V_{brine}}$) represents the volume of brine and surfactant mixed together in one phase which can be expressed as shown in **Equation 26**:

Equation 38

$$V_{brine} = V_{pore} - \frac{(m_{surfactant\ flooding} - m_{dry\ core} - \rho_{brine} V_{pore})}{(\rho_{oil} - \rho_{brine})}$$

Now, the residual oil saturation, the water saturation and the recovery can be calculated.

Let:

$\mathbf{S_{or}}$: Residual Oil Saturation

$\mathbf{S_{w}}$: Water Saturation

The irreducible oil saturation ($\mathbf{S_{or}}$) is given by **Equation 39**:

Equation 39

$$S_{or} = \frac{V_{oil}}{V_{pore}}$$

The water saturation (**S $_w$**) is given by **Equation 40**:

Equation 40

$$S_w = \frac{V_{brine}}{V_{pore}} = 1 - S_o$$

Next the recovery must be calculated. To calculate the recovery, we must know the volume of the oil recovered due to surfactant flooding. The volume of the oil that was expelled from the rock (**ΔV_{oil}**) can be found by subtracting the volume of the oil inside the core after surfactant flooding (**$V_{oil\ surfactant\ flooding}$**) from the volume of oil inside the core after waterflooding (**$V_{oil\ waterflooding}$**). The volume of oil expelled by surfactant flooding is given by **Equation 41**.

Let:

ΔV_{oil} : Volume of the oil that was expelled (cc)

$V_{oil\ surfactant\ flooding}$: The volume of oil inside core following surfactant flooding recovery (cc)

$V_{oil\ waterflooding}$: The volume of oil inside core following waterflooding recovery (cc)

Equation 41

$$\Delta V_{Oil} = V_{oil\ waterflooding} - V_{oil\ surfactant\ flooding}$$

Therefore, the recovery (**R**) can be calculated through **Equation 42**:

Equation 42

$$R\ (\%\ of\ OIP) = \frac{\Delta V_{oil}}{V_{oil\ waterflooding}} \qquad OR \qquad R\ (\%\ of\ OOIP) = \frac{\Delta V_{oil}}{V_{oil\ initial}}$$

4.2 Case 2: Fractured Carbonate Samples

For the theory section in Case 2, the parameters in **Table 4** of Case 1 will be re-defined to match the following case. Again, these parameters will define the mass of the core throughout the transitional stages of the experimental procedure. An 'f' subscript will denote a fractured core. There are five stages at which the mass of the fractured core was recorded. Please note that these masses were not necessarily obtained in this order. These stages are summarized in the **Table 5** below.

Table 5. Mass of the Core at Different Stages of the Experiment for Case 2

Stage	Nomenclature	Mass	Core Sample Contents
1	$m_{f\ dry}$	Fractured dry core sample	NA
2	$m_{f\ brine\ saturated}$	Fractured core sample after brine saturation	Brine
3	$m_{f\ (brine + oil)\ saturated}$	Fractured core sample after decane oil saturation	Brine n-Decane
4	$m_{f\ waterflooding}$	Fractured core sample after primary recovery, waterflooding	Brine n-Decane
5	$m_{f\ foam\ flooding}$	Fractured core sample after secondary recovery, foam flooding	Brine n-Decane Foam
6	$m_{f\ post\ foam\ water\ flooding}$	Fractured core sample after post foam waterflooding	Brine n-Decane Foam

Calculations will be discussed below in the same order as Case 1, which does not exactly match the order of the experiment for Case 2.

4.2.1 Porosity Calculations

Compared to Case 1, an alteration in porosity is to be expected in FD3H and FD4H due to the following:

i. Lost rock fragments during the creation of the fracture - lost pore volume
ii. Additional porosity due to the fracture

Again, porosity is defined as the ratio of pore volume to bulk volume. Therefore, both the pore volume and the bulk volume must be obtained. Bulk volume (**V_{bulk}**) is defined as the product of the cross-sectional area **(A_{cs}**) by the core length (**L**).

Equation 43

$$V_{bulk} = A_{cs}L \quad \rightarrow \quad V_{bulk} = \left(\frac{\pi d^2}{4}\right)L$$

After the bulk volume for both samples were calculated, the difference between the brine saturated core mass (**$m_{f\ brine\ saturated}$**) and the dry core mass (**$m_{f\ dry}$**) was calculated, delta mass (**Δm**).

Equation 44

$$\mathbf{\Delta m} = m_{f\ brine\ saturated} - m_{f\ dry}$$

This difference in mass (**Δm**) represents the mass of the brine within the rock sample and the fracture filling. When this mass is divided by the density of brine (**ρ_{brine}**) the volume of brine (**V_{brine}**) is obtained. If the core is fully saturated, it can be assumed that volume of brine is equal to the pore volume (**V_{pore}**).

Equation 45

$$\therefore V_{pore} = V_{brine} = \frac{\Delta m}{\rho_{brine}}$$

Dividing the pore volume by the bulk volume, the porosity of the core is obtained

Equation 46

$$\therefore \ \Phi = \ \frac{V_{pore}}{V_{bulk}}$$

4.2.2 Saturation Calculations

The initial oil saturation (**S_o**) and the irreducible water saturation (**S_{wr}**) were calculated after the brine saturated core was flooded with oil. Again, the brine and decane saturation was done *before* the core was fractured to ensure that they filled the pore spaces rather than bypassing through the fracture. Following oil flooding, the core was fractured. This corresponds to Stage 3 in **Table 5**. The fractured core sample mass after oil flooding is given by (**$m_{f\ (brine\ +\ oil)\ saturated}$**). Next, the volume of oil (**V_{oil}**) and brine (**V_{brine}**) was calculated through material balance.

The total core mass at stage 3 (**$m_{f\ (brine\ +\ oil)\ saturated}$**) is a sum of the dry core mass (including jacketing and fracture filling), plus the mass of the oil and brine inside. Therefore, the total mass of the core at the end of stage 3 is given by **Equation 47**.

Equation 47

$$m_{\,f\ (brine+oil)\ saturated} = \ m_{f\ dry\ core} \ + \ m_{\,oil} \ + \ m_{\,brine}$$

The same methodology as in Case 1 is used to determine the volume of oil (**V_{oil}**). The intermediate steps have hence been skipped to the final result (**Equation 48)**:

Equation 48

$$V_{\,oil} = \frac{(m_{\,f\ (brine+oil)\ saturated} - m_{f\ dry\ core} - \rho_{\,brine} V_{\,pore})}{(\,\rho_{\,oil} - \ \rho_{\,brine}\,)}$$

The volume of brine (**V brine**) can be expressed as shown in **Equation 49**:

Equation 49

$$V_{brine} = V_{pore} - \frac{(m_{f\,(brine+oil)\,saturated} - m_{f\,dry\,core} - \rho_{brine} V_{pore})}{(\rho_{oil} - \rho_{brine})})$$

Now, the initial oil saturation and the irreducible water saturation can be calculated in the same way. The initial oil saturation (**S o**) is given by **Equation 50**:

Equation 50

$$S_o = \frac{V_{oil}}{V_{pore}}$$

The irreducible water saturation (**S wr**) is given by **Equation 51**:

Equation 51

$$S_{wr} = \frac{V_{brine}}{V_{pore}} = 1 - S_o$$

4.2.3 Secondary Recovery Calculation: Waterflooding

Following brine saturation, decane saturation and fracturing, the core samples were now ready for waterflooding. Calculations were done after waterflooding to calculate the reducible oil saturation (**S or**), the water saturation (**S w**), and the recovery (**R**). Following waterflooding, Stage 4 **Table 6**5 the core, containing oil and brine, was weighed. The fractured core sample mass after waterflooding is given by (**m f waterflooding**). Again, material balance calculations were re-applied to determine the new volume of oil (**V oil**), the new volume of brine (**V brine**), and the volume of oil recovered (**R**).

The total fractured core mass at stage 4 (**m f waterflooding**) is a sum of the dry core mass (including jacketing and fracture filling), the mass of the oil and the mass of brine. Therefore, the total mass of the core at the end of stage 4 is given by **Equation 52**.

Equation 52

$$m_{f\ waterflooding} = m_{f\ dry\ core} + m_{oil} + m_{brine}$$

The same methodology as in Case 1 is used to determine the volume of oil (**V_{oil}**). The intermediate steps have hence been skipped to the final result (**Equation 53)**:

Equation 53

$$V_{oil} = \frac{(m_{f\ waterflooding} - m_{f\ dry\ core} - \rho_{brine} V_{pore})}{(\rho_{oil} - \rho_{brine})}$$

And the volume of brine (**V_{brine}**) can be expressed as shown in **Equation 54**:

Equation 54

$$V_{brine} = V_{pore} - \frac{(m_{f\ waterflooding} - m_{f\ dry\ core} - \rho_{brine} V_{pore})}{(\rho_{oil} - \rho_{brine})})$$

Now, the residual oil saturation, the water saturation and the recovery are calculated. The residual oil saturation (**S_{or}**) is given by **Equation 55***:*

Equation 55

$$S_o = \frac{V_{oil}}{V_{pore}}$$

The water saturation (**S_w**) is given by **Equation 56**:

Equation 56

$$S_w = \frac{V_{brine}}{V_{pore}} = 1 - S_o$$

Next the recovery needs to be calculated. The same methodology as in Case 1 is used to determine oil recovery (**R**). The intermediate steps have hence been skipped to the final result (**Equation 57):**

Equation 57

$$R = \frac{\Delta V_{oil}}{V_{oil\ initial}}$$

For waterflooding, this recovery represents the recovery as a % of the OIP (oil in place) as well as the recovery as a % of the OOIP (original oil in place).

4.2.4 Tertiary Recovery Calculation: Foam Flooding

Following brine saturation, decane saturation and waterflooding (secondary recovery), tertiary recovery (foam flooding followed by waterflooding) was carried out.

4.2.4.1 Foam Injection

Once the foam flooding experiment (Stage 5, **Table 5**) is complete, the fractured core containing oil, brine and foam was weighed. The core sample mass after foam flooding is given by (**m f foam flooding**). The total core mass at stage 5 (**m f foam flooding**) is a sum of the dry core mass and the mass of the oil, brine as well as foam inside. In this case the foam density is not equal to the brine density, and thus the equation will not reduce to two unknowns as in the case of surfactant flooding. This time we will have three unknowns and only two equations. Therefore, recovery calculations will not be conducted until after water injection. Only the weight (**m f foam flooding**) will be recorded. The total mass of the core at the end of stage 5 is given by **Equation 58**.

Equation 58

$$m_{f\ foam\ flooding} = m_{f\ dry\ core} + m_{oil} + m_{brine} + m_{foam}$$

4.2.4.2 Post Foam Brine injection

Following brine saturation, decane saturation, fracturing and foam flooding the core samples were now ready for the final flooding experiment: Post foam waterflooding. It is assumed that eventually brine will flush all the foam out of the core leaving brine and decane only. Therefore, the following calculations will assume that the core contains brine and decane only. Following the injection of brine (sweeping fluid), Stage 6 in **Table 5**, the core was weighed (**$m_{f\ post\ foam\ waterflooding}$**). Again, material balance calculations were re-applied to determine the new volume of oil (**V_{oil}**) and the new volume of brine (**V_{brine}**) within the core.

The total core mass at stage 6 (**$m_{f\ post\ foam\ waterflooding}$**) is a sum of the dry core mass (including jacketing and fracture filling), the mass of the oil and the mass of brine. Therefore, the total mass of the core at the end of stage 6 is given by **Equation 59**.

Equation 59

$$m_{f\ post\ foam\ waterflooding} = m_{f\ dry\ core} + m_{oil} + m_{brine}$$

The same methodology as in Case 1 is used to determine the volume of oil (**V_{oil}**). The intermediate steps have hence been skipped to the final result:

Equation 60

$$V_{oil} = \frac{(m_{f\ post\ foam\ waterflooding} - m_{f\ dry\ core} - \rho_{brine} V_{pore})}{(\rho_{oil} - \rho_{brine})}$$

And the volume of brine (**V_{brine}**) can be expressed as shown in **Equation 61**:

Equation 61

$$V_{brine} = V_{pore} - \frac{(m_{f\ post\ foam\ waterflooding} - m_{f\ dry\ core} - \rho_{brine} V_{pore})}{(\rho_{oil} - \rho_{brine})})$$

Now, the residual oil saturation, the water saturation and the recovery are calculated. The residual oil saturation (**S_{or}**) is given by **Equation 62***:*

Equation 62

$$S_o = \frac{V_{oil}}{V_{pore}}$$

The water saturation (**S_w**) is given by **Equation 63**:

Equation 63

$$S_w = \frac{V_{brine}}{V_{pore}} = 1 - S_o$$

Next the recovery for the entire tertiary recovery process must be calculated. To calculate the recovery, we must know the volume of the oil expelled from the rock (**ΔV_{oil}**) which equals the volume of the oil inside the core after waterflooding (**$V_{oil\ post\ foam\ waterflooding}$**) minus the initial oil volume (**$V_{oil\ initial}$**) of the core. The volume of oil expelled by waterflooding is given by **Equation 64**.

Let:

ΔV_{oil} : Volume of the oil that was expelled (cc)

$V_{oil\ initial}$: The initial volume of oil inside the core before any recovery (cc)

$V_{oil\ post\ foam\ waterflooding}$: The volume of oil inside core following waterflooding recovery (cc)

Equation 64

$$\Delta V_{Oil} = V_{oil\ initial} - V_{oil\ \text{post foam}\ waterflooding}$$

Therefore, the recovery (**R**) can be calculated through **Equation 65**:

Equation 65

$$R\ (\%\ of\ OIP) = \frac{\Delta V_{oil}}{V_{oil\ waterflooding}} \qquad OR \qquad R\ (\%\ of\ OOIP) = \frac{\Delta V_{oil}}{V_{oil\ initial}}$$

CHAPTER V

RESULTS AND DISCUSSION

In this chapter, the results and figures are displayed for both Case 1, non-fractured core samples, and Case 2, fractured core samples. Case 1 will display core parameters, porosity, permeability, oil flooding, waterflooding and surfactant flooding results, and Case 2 will display the same, except surfactant flooding will be substituted with foam flooding.

For the first two sections of results, core measurements and porosity, the results will be summarized in tabulated form for both cases. The porosity results will be split into two parts for Case 1: Porosity results obtained through Archimedes method (Experimental Method 1) and porosity results obtained from thin section analysis (Experimental Method 2). In case 2, porosity results were only derived by Archimedes method.

Following porosity results, permeability results will be discussed for Case 1. A graph of Q vs. ΔP will be depicted for a set of flowrates, from which permeability will be estimated using Darcy's law. For Case 2, no permeability results were obtained due to the complexities of estimating the permeability in fractured media. These complexities occur due the fact that two separate permeability values must now be considered: the fracture permeability and the rock permeability.

Following the discussion of permeability, oil flooding results will be discussed. For both Case 1 and Case 2, two plots will be presented. The first plot will depict time vs. pressure drop, and second plot will depict number of pore volumes injected vs. pressure drop. From these plots, the breakthrough times will be identified and the graph trends will be discussed. The properties of the core following decane flooding will be summarized in tabulated form indicating the core's initial oil and irreducible water saturations.

Next, the results of improved oil recovery will be displayed. Again, the same plots will be presented in both cases for waterflooding injection as was previously done in oil flooding. The results summarizing the core properties following waterflooding will be tabulated in the exact same way as before. This time, the table will include parameters such as the water saturation, the residual oil saturation, the volume of oil expelled out of the rock due to waterflooding and the recovery.

Finally, enhanced oil recovery results will be displayed for both Case 1 and Case 2. For Case 1 surfactant flooding results will be displayed. Again, time and injected pore volume plots vs. pressure drop will be displayed along with the breakthrough times. A table will be presented to summarize the additional recovery obtained by surfactant flooding, highlighting important parameters such as water saturation, residual oil saturation, the volume of oil expelled due to surfactant flooding, and the recovery. For Case 2, foam flooding results will be displayed. Again, a plot of time vs. pressure drop was obtained. This plot was obtained only for one core, out of two samples, due to a failed quality check for the first. Similarly, a table will be presented to summarize the additional recovery obtained by foam flooding, highlighting important parameters such as water saturation, residual oil saturation, the volume of oil expelled due to foam flooding, and the recovery.

5.1 Case 1: Non-Fractured Carbonate Samples

5.1.1 Core Parameters

Table 6 below presents the initial core parameters. The parameters include length, diameter, cross sectional area, bulk volume and dry mass.

Table 6. Core Parameters

Core Sample	Length L	Diameter D	Cross Section Area A_{cs}	Bulk Volume V_{bulk}	Dry Mass m_{dry}
	cm	*cm*	cm^2	*cc*	*g*
FD3H	12.93	3.78	11.25	145.41	329.38
FD4H	13.09	3.78	11.22	146.87	334.25
FD5C	12.98	3.77	11.14	144.7	300.27

From **Table 6** it can be observed that the three cores are almost identical in dimensions, with FD4H being the heaviest, followed by FD3H, and then FD5C.

5.1.2 Porosity

The porosity results will be split into two parts; porosity results obtained through Archimedes' method, and porosity results obtained though thin section analysis.

5.1.2.1 Experimental Method 1 – Archimedes' Method

This first experimental method is based on Archimedes' method of weights as explained in the theory section. **Table 7** below summarizes the porosity results for the three core samples using Archimedes' method.

Table 7. Porosity Values obtained through Archimedes' Method

Core Sample	Brine Saturated Mass $m_{brine\ saturated}$	(Brine saturated mass- Dry mass) Δm	Volume of Pores V_{pore}	Bulk Volume V_{bulk}	Porosity Φ
	G	*g*	*cc*	*Cc*	*%*
FD3H	348.59	19.21	18.83	145.41	13
FD4H	353.63	19.38	19	146.87	13
FD5C	330.91	30.64	30.04	144.7	21

From **Table 7**, it can be concluded that calculations show that FD5C has the largest pore volume (30.64 cc) and porosity (21%). FD3H and FD4H have almost identical porosities (13%) and pore volumes (19 cc).

5.1.2.2 Experimental Method 2 – Thin Section Analysis

The second experimental method is based on porosity estimation from the rock's thin section analysis. Three arbitrary images were selected from the thin section taken (sample FD3H) for the purpose of the analysis. Rock Image 1, Rock Image 2 and Rock Image 3 are shown below in **Figure 9**, **Figure 10** and **Figure 11** respectively.

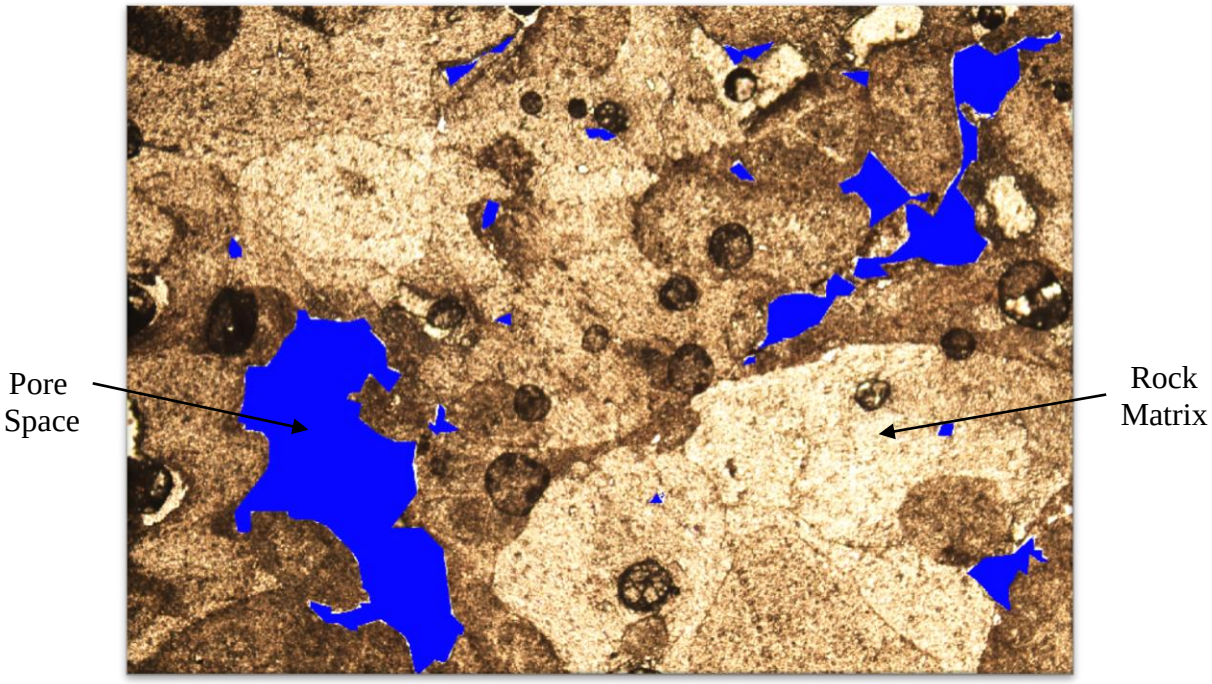

Figure 9. FD3H Rock Image 1

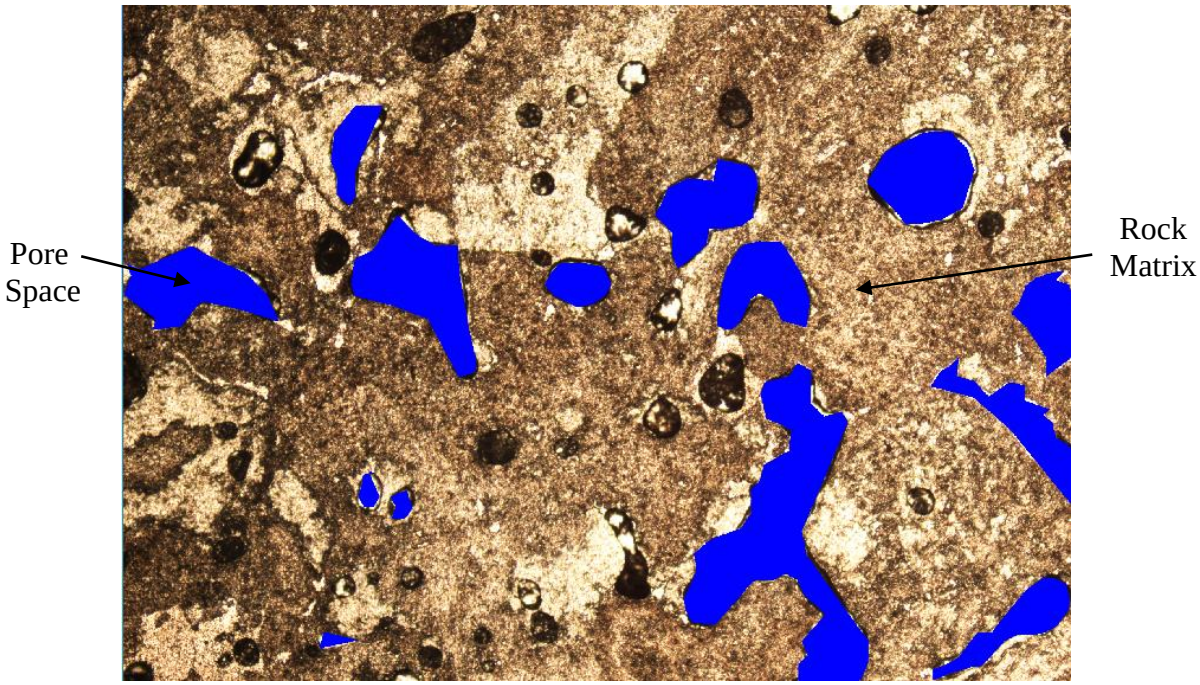

Figure 10. FD3H Rock Image 2

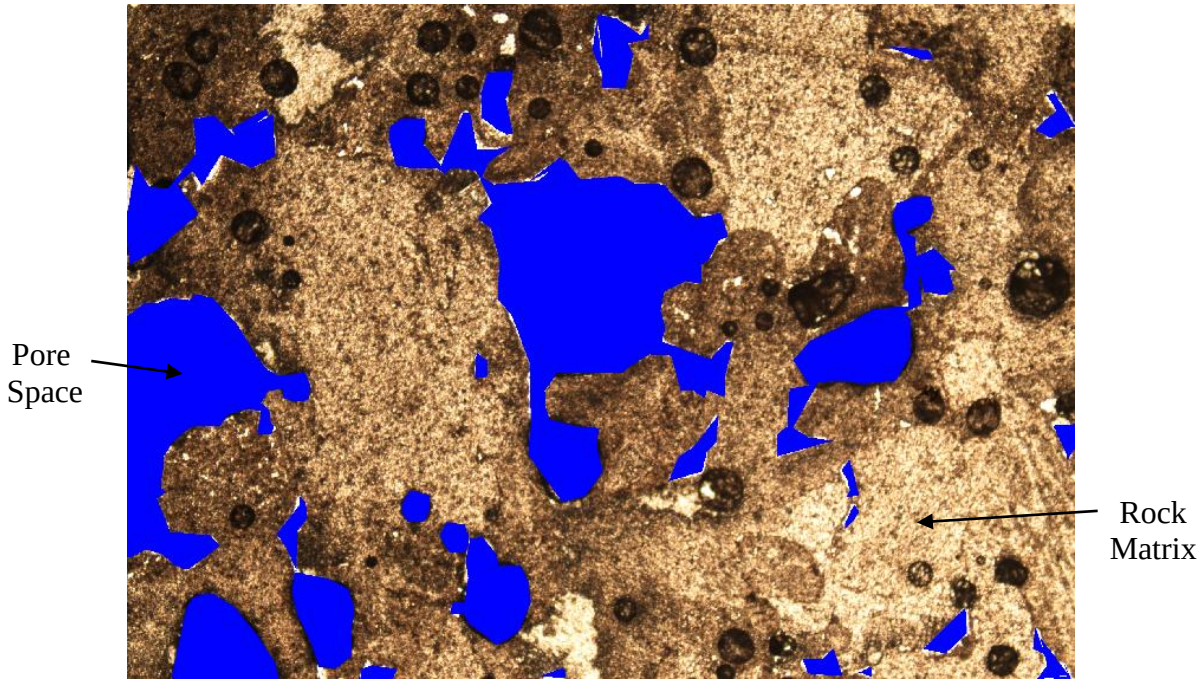

Figure 11. FD3H Rock Image 3

In the above figures the pore volumes are shaded in blue. Identification of the pore space was required by the MATLAB code in order for it to estimate the porosity. **Table 8** below summarizes the porosity values obtained from each of the thin section images shown above and presents the calculated average porosity obtained based on the porosity values predicted from each image.

Table 8. Porosities Values obtained through Thin Section Analysis

Image sample	Porosity Φ	Average Porosity $\Phi_{avg.}$
	%	%
1	9.07	12.92
2	11.67	
3	18.03	

From **Table 8**, rock Image 1 was estimated to have a porosity of 9. 07 %, rock image 2 was estimated to have a porosity of 11. 67 % and rock image 3 was estimated to have a porosity of 18. 03 %. This yields an average porosity of 12. 92 %. Three images were taken for experimental reliability for the porosity calculation. This is especially essential in our case since carbonate rocks are heterogeneous and porosity distributions vary greatly throughout the core sample.

5.1.2.3 Comparison of Methods

Table 9 below summarizes and compares the porosity values obtained from Archimedes' method (Experimental Method 1) and thin section analysis method (Experimental Method 2).

Table 9. A Comparison of the Porosity values obtained through both Methods

Experimental Method 1: Thin Section Analysis Method	*Experimental Method 2:* Archimedes' Method	Comparison of Methods
Average Porosity Φ avg.	Porosity Φ	% Difference Δ
12.92%	13%	0.59%

Using thin section analysis, a porosity of 12.92 % was obtained for sample FD3H. Using Archimedes' method, a porosity of 13 % was obtained for the same rock. The percentage difference between both methods is 0.59 %. This difference is less than 1 % portraying an almost perfect match of results. This greatly increases the reliability of the upcoming sections which rely on accurate measurement of porosity and pore volume.

5.1.3 Permeability

As discussed in the theory section, permeability calculations were conducted through a series of brine flooding experiments followed by application of Darcy's Law. For detailed calculation please refer to Chapter III.

Figure 12 below displays the plot of pressure drop across the core vs. the injected brine flowrate. For each core sample, the flowrate was altered three times. Once a plot was obtained, as shown below, the slopes were used for calculating the permeability.

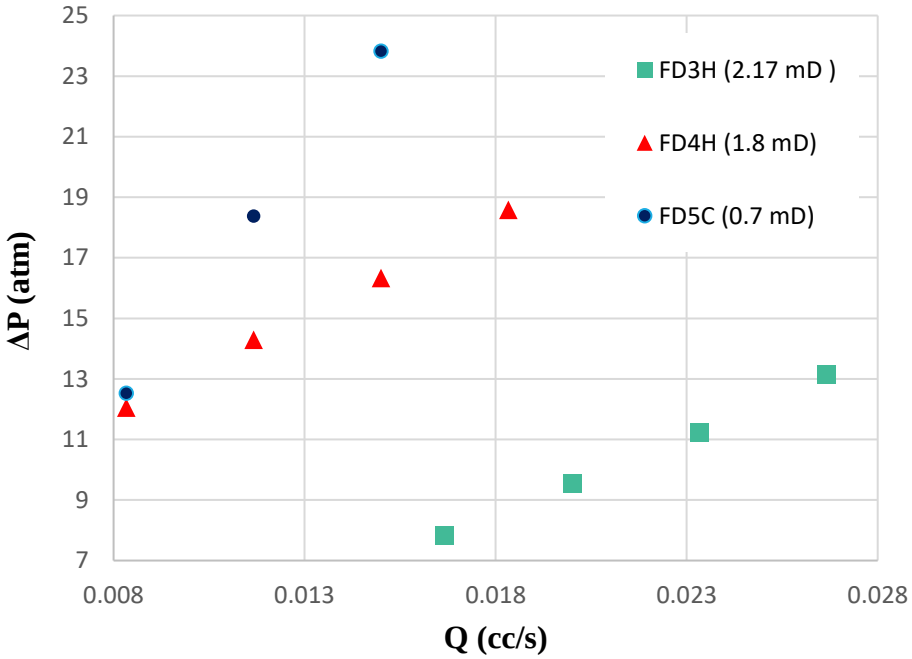

Figure 12. ΔP (atm.) vs. Q (cc/s) for Permeability Estimation

The general trend that can be observed is that as the flowrate (Q) is increased, the pressure drop (ΔP) also increases linearly. All three samples exhibit the same trend, with sample FD5C experiencing the greatest increase in pressure drop for a specified increase in flowrate. That is, FD5C has the steepest slope, followed by FD4H and then FD3H. The steepest slope also correlates

to the lowest permeability. This is because Darcy's law states that $Q = \frac{k\,A_{cs}}{u\,L}\,(\Delta p)$. If we re-arrange this into the form of a straight line equation, where Δp represents y, Q represents x, $\frac{u\,L}{k\,A_{cs}}$ represents m, and the intercept c = 0, we get $\Delta p = \left(\frac{u\,L}{k\,A_{cs}}\right) Q \rightarrow y = mx + c$. Where the slope (m) is given by $\frac{k\,A_{cs}}{u\,L}$. If we re-arrange this for the permeability k, we find $k = \frac{\mu\,L}{(slope)A_{cs}}$. Therefore it makes sense that as the slope increases (becomes more steep) the permeability decreases. Thus, FD3H has the highest permeability, followed by FD4H and then FD5C. **Table 10** below summarizes the permeability results for the three core samples.

Table 10. Permeability Values of Core Samples

Sample	Permeability *mD*
FD3H	2.17
FD4H	1.8
FD5C	0.7

As we can see from the table above, all core samples are extremely tight with very low permeability values. FD3H has the highest permeability (2.17 mD), followed by FD4H (1.8 mD), then FD5C (0.7 mD). Despite the fact that FD5C has the highest porosity of the three (21%), it has the lowest permeability (0.7 mD).

5.1.4 Oil flooding

The first of the flooding procedures to take place was decane oil flooding. Again, the details of this process and the calculations are described in earlier sections. A real time plot of the pressure drop across the core vs. the elapsed time was plotted for all three samples. Similarly, the same was done as a function of the number of injected pore volumes of decane. **Figure 13** below shows a plot of the pressure drop vs. elapsed time for FD3H, FD4H and FD5C, and **Figure 14** depicts the same but as function of number of injected pore volumes

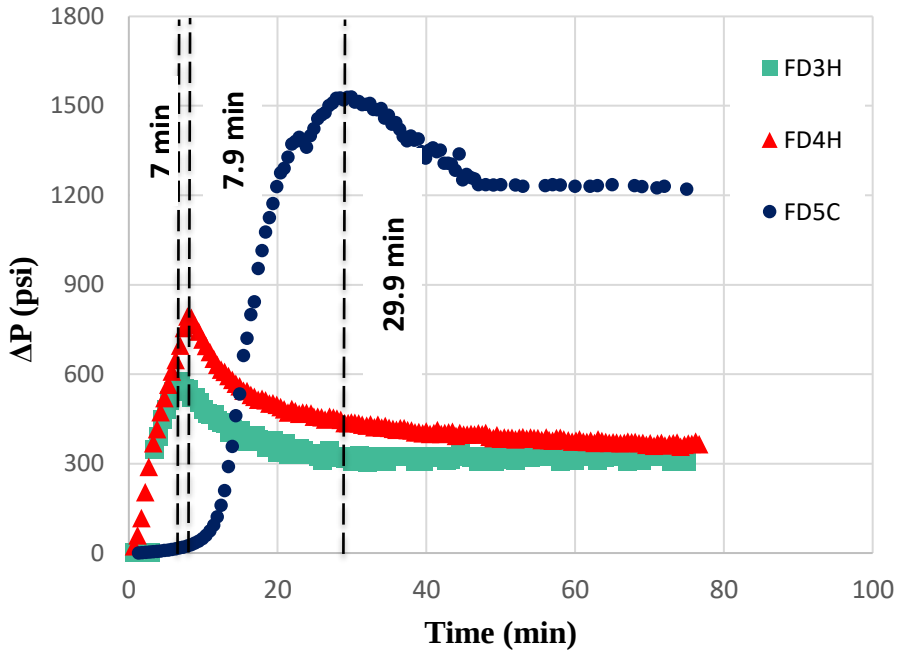

Figure 13. Decane flooding - ΔP (psi) vs. Time (min) – Case 1

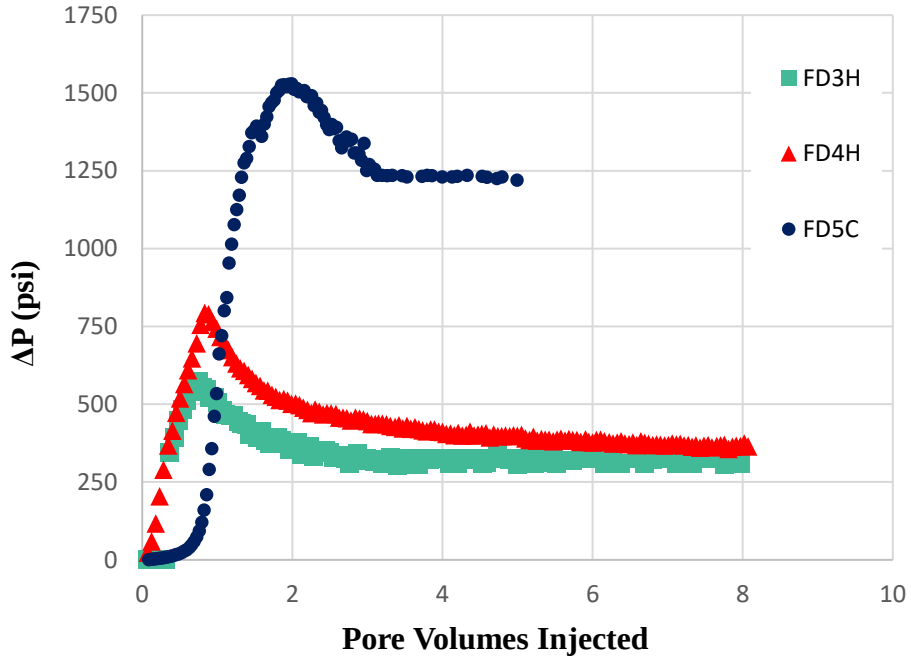

Figure 14. Decane flooding - ΔP (psi) vs. Number of Pore Volumes Injected – Case 1

From both **Figure 13** and **Figure 14** we can see that there is a sharp increase in the pressure drop prior to breakthrough and then a steady decrease to plateau after breakthrough is reached. The initial increase in pressure can be attributed to the compression of the fluid within the system during decane injection. The pressure will continue to increase due to the greater rate of fluid inflow into the core compared to the fluid outflow out of the core. Once breakthrough point is reached, this is the point at which the first drop of decane is observed to leave the core. Compression effects become less significant and viscosity effects take over. At this point, it is expected that viscous fingering has occurred between the less viscous decane and the brine resulting in an earlier breakthrough. This means that at the time of breakthrough there is still a significant amount of reducible brine remaining in the core. Therefore, as more brine leaves the core and as more decane saturates the core, the average viscosity of the fluid within the core

decreases (decane viscosity is less than brine viscosity). By Darcy's Law, the reduction in the overall viscosity leads to a reduction in pressure. Once steady state is reached, the maximum possible oil saturation under these conditions is approached.

A couple of observations can be noted by comparing the different trends between the three core samples. In the above figures the trends are highlighted in green for FD3H, in red for FD4H and in blue for FD5C. Sample FD3H has the steadiest increase in pressure drop, followed by FD4H, and then FD5C, an outlier, with a very rapid increase in pressure drop. This trend can be explained by the inverse relationship between permeability (k) and pressure drop (ΔP) in Darcy's law, assuming all other parameters are kept constant. Since FD5C has the lowest permeability, it experiences the highest pressure drop, and since FD3H has the highest permeability, it experiences the smallest pressure drop. However in all cases the relatively sharp increase in pressure drop can be attributed to the low permeability nature of the samples (< 2 mD).

A final observation on breakthrough times can be made from the figures above. FD5C has the longest breakthrough time (30 minutes.), followed by FD4H (7.9 minutes) and finally FD3H (7minutes). These breakthrough times are again a function of permeability. The higher the permeability, the lower the breakthrough time. Since FD3H has the highest permeability, followed by FD4H, and then FD5C, FD3H in turn has the shortest breakthrough time followed by FD4H and then FD5C. **Table 11** below summarizes the breakthrough times of each of the three core samples.

Table 11. Breakthrough Times of Core Samples following Decane Flooding - Case 1

Core Samples	Breakthrough Time *min*	Permeability mD
FD3H	7	2.17
FD4H	7.9	1.8
FD5C	29.9	0.7

Table 12 below summarizes the core properties after decane flooding was complete and the samples were weighed.

Table 12. Core Properties following Oil Flooding - Case 1

Core Sample	Brine/ Decane Saturated Mass $m_{(brine + oil) saturated}$	Volume of Oil V_{oil}	Volume of Brine V_{brine}	Oil Saturation S_o	Residual Water Saturation S_{wr}
	g	*cc*	*cc*		
FD3H	345.15	11.86	6.97	0.63	0.37
FD4H	350.93	9.32	9.68	0.49	0.51
FD5C	324.47	22.21	7.83	0.74	0.26

Table 12 above shows the mass after decane flooding (**$m_{(brine + oil) saturated}$**), the volume of oil within the rock (**V_{oil}**), the volume of brine within the rock (**V_{brine}**), the initial oil saturation (**S_o**) and the irreducible water saturation (**S_{wr}**). For example, one can quickly tell that sample FD5C had the highest initial oil saturation ($S_o = 0.74$), whereas FD4H had the lowest initial oil saturation ($S_o = 0.49$).Detailed calculations of how these values were derived from the measured weights, using material balance, are discussed above in Chapter III. These parameters now describe a core containing both brine and decane, thus representing reservoir conditions.

5.1.5 Waterflooding

The first of the recovery procedures to take place following brine and decane saturation is waterflooding. Again, the details of this process and the calculations are described in earlier sections. A real time plot of the pressure drop across the core vs. the elapsed time was plotted for all three samples. Similarly, the same was done as a function of the number of injected pore volumes of decane. **Figure 15** below shows a plot of the pressure drop vs. elapsed time for FD3H, FD4H and FD5C, and **Figure 16** depicts the same but as function of number of injected pore volumes.

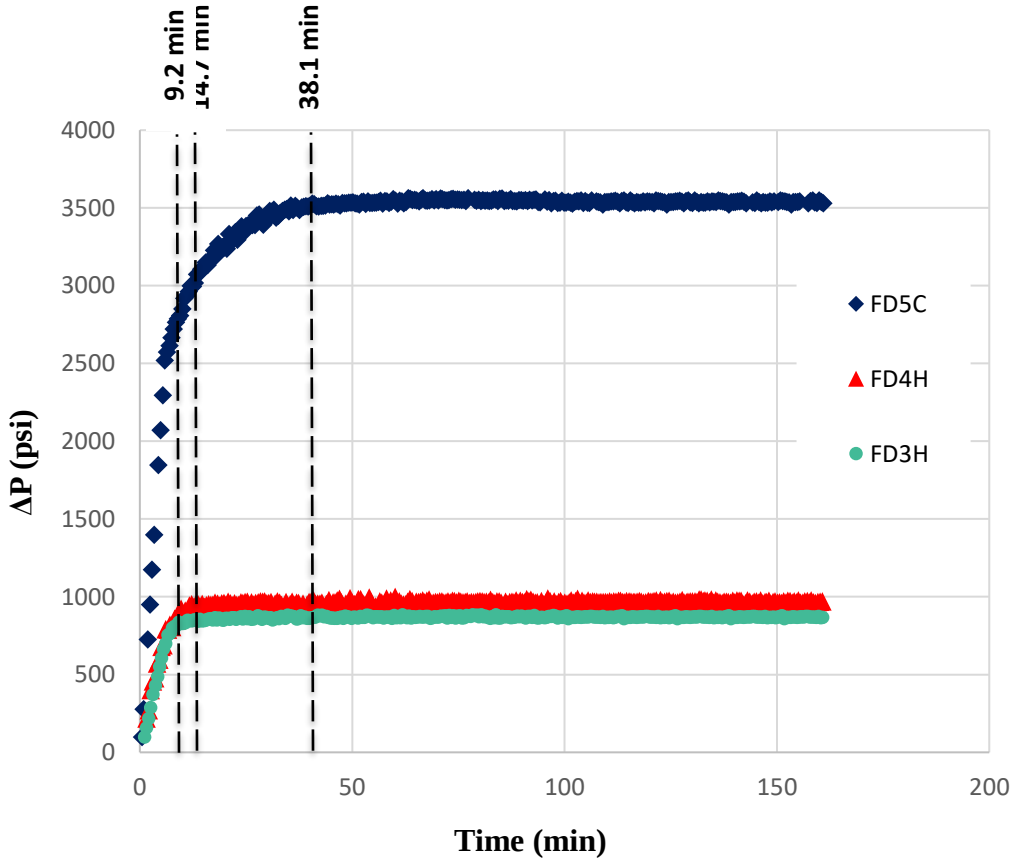

Figure 15. Waterflooding - ΔP (Psi) vs. Time (min) - Case 1

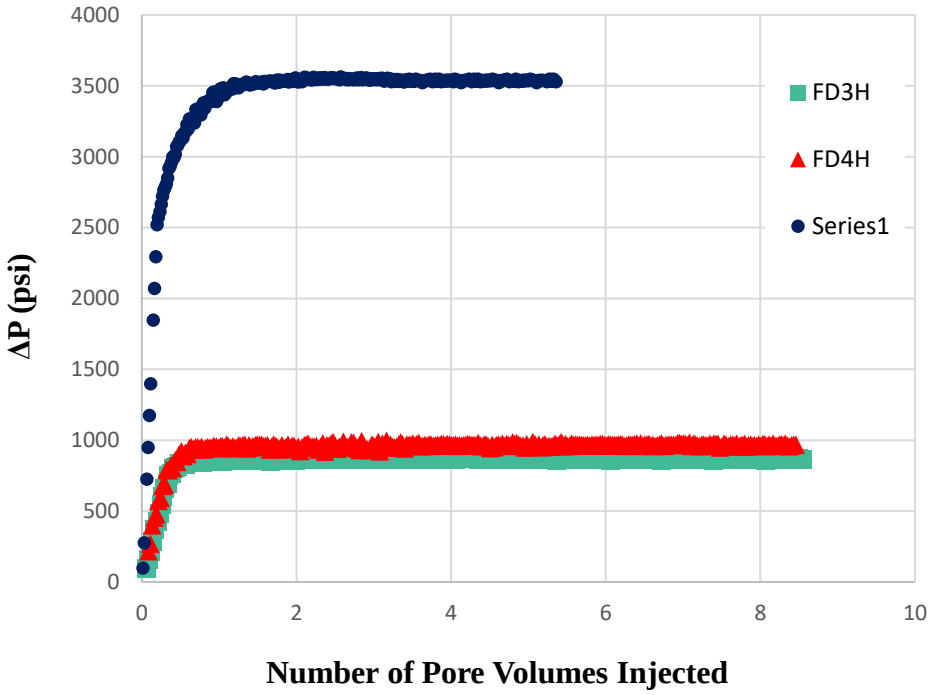

Figure 16. Waterflooding - ΔP (Psi) vs. Number of Pore Volumes Injected - Case 1

From both **Figure 15** and **Figure 16** we can see that there is a sharp increase in the pressure drop prior to breakthrough and then a steady plateau after breakthrough is reached. As brine is injected, the pressure increases due to compressibility effect. The pressure will continue to increase due to the greater rate of fluid inflow into the core compared to fluid outflow out of the core. Once breakthrough point is reached, this is the point at which the first drop of brine is observed to leave the core. Compression effects become less significant and viscosity effects take over. Because we are displacing a lower viscosity fluid (decane) with a higher viscosity fluid (brine), the effects of viscous fingering are not severe, thus the drop in pressure observed in decane flooding is not observed here. At breakthrough here the vast majority of decane has already been displaced and hence average viscosity remains almost constant. Hence, by Darcy's law the pressure drop reaches a steady state.

A couple of observations can be noted by comparing the different trends between the three core samples. The same color key is used to identify the cores. Again, sample FD3H has the steadiest increase in pressure drop, followed by FD4H, and then FD5C, an outlier, with a very rapid increase in pressure drop. This trend can be explained by the inverse relationship between permeability (k) and pressure drop (ΔP) in Darcy's law, assuming all other parameters are kept constant.

A final observation on breakthrough times can also be drawn from the figures above. FD5C has the longest breakthrough time (38.1 minutes.), followed by FD4H (14.7 minutes) and finally FD3H (9.2 minutes). These breakthrough times are again a function of permeability. The higher the permeability, the lower the breakthrough time. Since FD3H has the highest permeability, followed by FD4H, and then FD5C, FD3H in turn has the shortest breakthrough time followed by FD4H and then FD5C. **Table 13** below summarizes the breakthrough times of each of the three core samples.

Table 13. Breakthrough Times of Core Samples following Waterflooding - Case 1

Core Samples	Breakthrough Time *min*	Permeability mD
FD3H	9.2	2.17
FD4H	14.7	1.8
FD5C	38.1	0.7

Table 14 below summarizes the core properties after waterflooding was complete and the samples were weighed.

Table 14. Core Properties following Waterflooding - Case 1

Core Sample	Core Mass after Waterflooding $m_{waterflooding}$	Volume of Oil V_{oil}	Volume of Brine V_{brine}	Residual Oil Saturation S_{or}	Water Saturation S_w	Volume of Oil expelled ΔV_{oil}	Recovery R
	g	*cc*	*cc*			*cc*	*%*
FD3H	346.14	8.45	10.38	0.45	0.55	3.41	28.78
FD4H	351.84	6.17	12.83	0.32	0.68	3.15	33.8
FD5C	326.89	13.86	16.18	0.46	0.54	8.34	37.58

Table 14 above shows the mass after waterflooding (**$m_{waterflooding}$**), the volume of oil within the rock (**V_{oil}**), the volume of brine within the rock (**V_{brine}**), the residual oil saturation (**S_{or}**), the water saturation (**S_w**), the volume of oil expelled due to waterflooding (**ΔV_{oil}**) and the percentage recovery obtained from waterflooding (**R**).

From Table 14, it can be concluded that secondary recovery was fairly efficient. The recovery due to waterflooding is in the range of 28 % to 38 %. FD5C had the highest recovery due to waterflooding (37.58 %) despite being the tightest sample (0.7 mD). Of an initial oil volume of 22.21 cc within the core, 8.34 cc were expelled due to waterflooding. The second highest recovery due to waterflooding was for sample FD4H (33.8 %). This sample had an initial oil saturation of 9. 32 cc. After waterflooding, 3.15 cc were expelled out of the rock. And finally, the core with the lowest recovery, (28.78 %), was sample FD3H. Of an initial 11.86 cc of oil within the core, 3.51 cc were expelled due to waterflooding. The high pressure drop applied and the delay in breakthrough time could be the cause of this. Detailed calculations of how these values were derived from the measured weights, using material balance, are discussed above in Chapter III

5.1.6 Surfactant Flooding

Following secondary recovery, enhanced oil recovery was implemented: surfactant flooding. Again, the details of this process and the calculations are described in earlier sections. A real time plot of the pressure drop across the core vs. the elapsed time was plotted for all three samples. Similarly, the same was done as a function of the number of injected pore volumes of decane. Note that the time shown on the plots have been adjusted for the plots and may not represent the full time of the test. **Figure 17** below is composed of two figures. The figure to the left shows a plot of the pressure drop vs. elapsed time for FD3H, FD4H and FD5C and the figure to the right shows the same plot, but enlarged for FD3H and FD4H alone. **Figure 18** depicts the same, but this time the pressure drop is a function of the number of injected pore volumes.

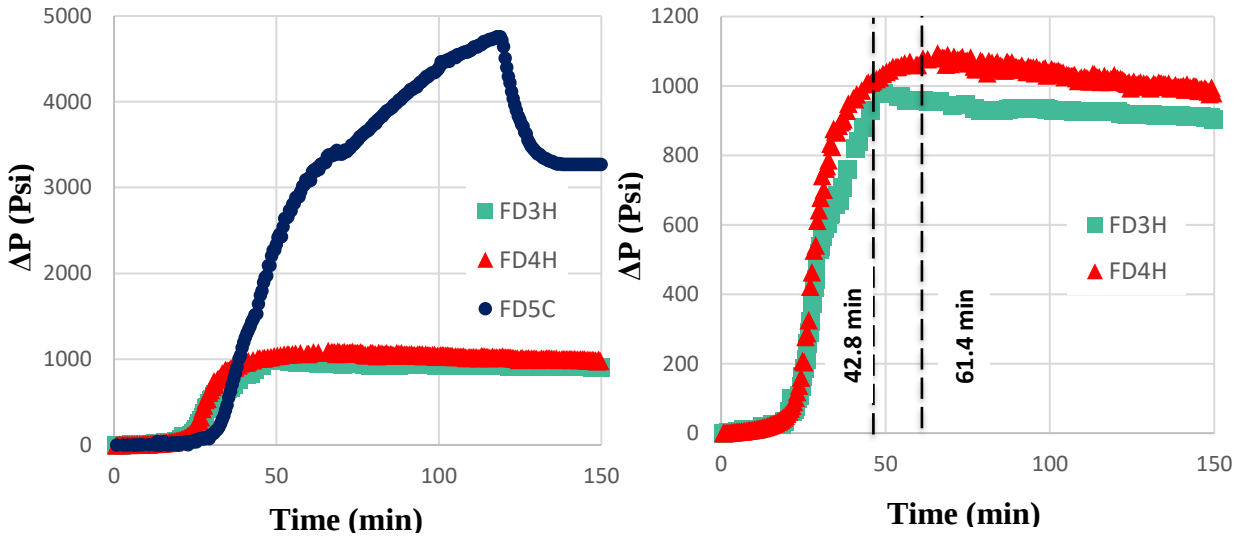

Figure 17. Surfactant flooding - ΔP (Psi) vs. Time (min) - Case 1

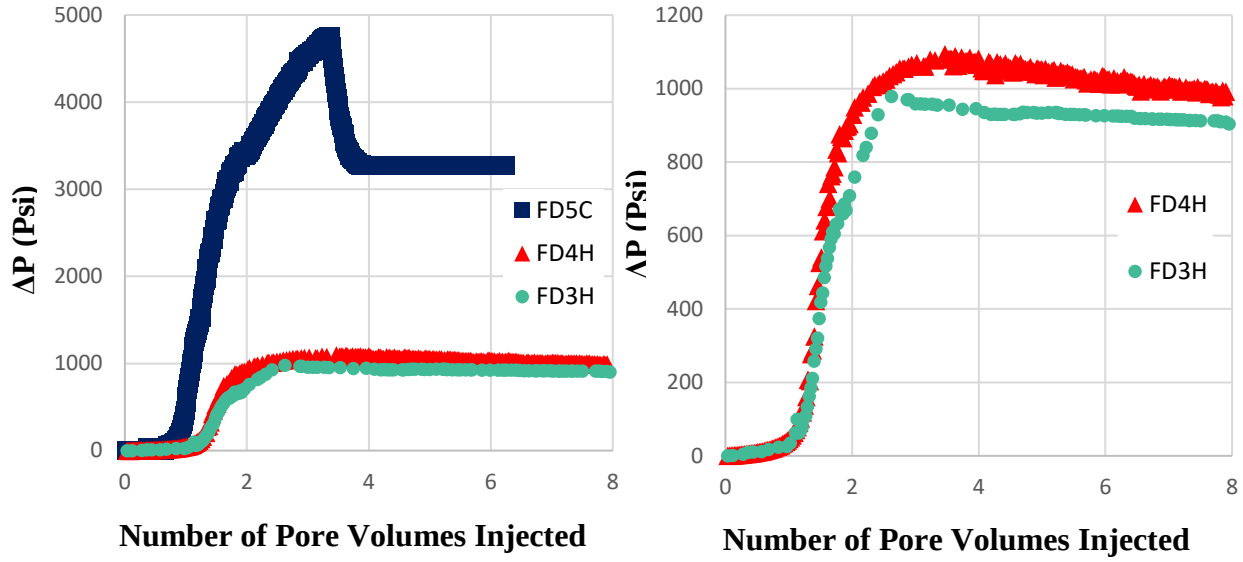

Figure 18. Surfactant flooding - ΔP (Psi) vs. Number of Pore Volumes Injected - Case 1

From both **Figure 17** and **Figure 18** the general trend for FD3H and FD4H is that there is a sharp increase in the pressure drop prior to breakthrough and then a very steady decrease after breakthrough. As for FD5C, an abnormal pressure trend is observed after t =100 minutes, where the pressure drop drops suddenly. Since this behavior is very different to the other two cores, some skepticism is placed on whether the marked breakthrough point identifies the breakthrough time. Most probably, the drop in pressure was due to core failure. Since this core had the lowest permeability, the pressure increase was high, and thus the overburden pressure was increased in accordance. This increase in overburden pressure could have caused failures/fractures in the rock as a result. Discussing the general trend of FD3H and FD4H, as surfactant is injected, the pressure increases due to the increased compression within the core. The pressure will continue to increase due to the greater rate of fluid inflow into the core compared to fluid outflow out of the core. Once breakthrough point is reached, this is the point at which the first drop of surfactant is observed to

leave the core. Compression effects become less significant and viscosity effects take over. Because we are displacing a lower viscosity fluid (mostly brine) with a higher viscosity fluid (surfactant), the effects of viscous fingering are not severe, thus the drop in pressure observed in decane flooding is not observed here. At breakthrough the vast majority of decane has already been displaced and hence the average viscosity remains almost constant. However the surfactant has also caused some changes in the rock wettability and interfacial tension making the fluid more mobile and causing the pressure drop to decrease in a steady manner as observed above.

A couple of observations can be noted by comparing the different trends between the three core samples. The same color key is used to identify the cores. Again, sample FD3H has the steadiest increase in pressure drop, followed by FD4H, and then FD5C, an outlier, with a very rapid increase in pressure drop. This trend can be explained by the inverse relationship between permeability (k) and pressure drop (ΔP) in Darcy's law, assuming all other parameters are kept constant.

A final observation on breakthrough times can be made from the Figures above. FD5C has the longest breakthrough time by far (118.9 minutes.), followed by FD4H (61.4 minutes) and finally FD3H (42.8 minutes). Again FD5C is an outlier. These breakthrough times are again a function of permeability. The higher the permeability, the lower the breakthrough time. Since FD3H has the highest permeability, followed by FD4H, and then FD5C, FD3H in turn has the shortest breakthrough time followed by FD4H and then FD5C. **Table 15** below summarizes the breakthrough times of each of the three core samples following surfactant flooding.

Table 15. Breakthrough Times of Core Samples following Surfactant Flooding - Case 1

Core Samples	Breakthrough Time *min*	Permeability mD
FD3H	42.8	2.17
FD4H	61.4	1.8
FD5C	118.9	0.7

Table 16 below summarizes the core properties after surfactant flooding was complete and the samples were weighed.

Table 16. Core Properties Following Surfactant Flooding - Case 1

Core Sample	Core Mass after Surfactant flooding	Volume of Oil	Volume of Brine	Residual Oil Saturation	Water Saturation	Volume of Oil expelled	Recovery	
	$m_{surfactant\ flooding}$	V_{oil}	V_{brine}	S_{or}	S_w	ΔV_{oil}	R	R
	g	*Cc*	*Cc*			*cc*	*%*	*% of OOIP*
FD3H	346.19	8.28	10.56	0.44	0.56	0.17	2.04	1.45
FD4H	351.85	6.14	12.86	0.32	0.68	0.03	0.56	0.37
FD5C	327.06	13.28	16.76	0.44	0.56	0.59	4.23	2.64

Table 16 above shows the mass of the cores after surfactant flooding (**$m_{surfactant\ flooding}$**), the volume of oil within the rock (**V_{oil}**), the volume of brine within the rock (**V_{brine}**), the residual oil saturation (**S_{or}**), the water saturation (**S_w**), the additional volume of oil expelled due to surfactant flooding (**ΔV_{oil}**) and the percentage recovery obtained from surfactant flooding (**R**). Please note that the core sample will also contain some surfactant inside. Since surfactant has the

same density as brine (1.02 g/cc), the notation "**V_{brine}**" will be used to refer to the 'mixture' of brine and surfactant left within the core.

From **Table 16**, it can be concluded that tertiary recovery surfactant flooding was efficient. The recovery due to surfactant flooding is in the range of 0.55-4.25 %. FD5C had the highest recovery due to surfactant flooding (4.23 %) despite being the tightest sample (0.7 mD). Of a residual oil volume of 13.86 cc left within the core after waterflooding, an additional 0.59 cc was expelled due to surfactant flooding. The high pressure drop applied and the delay in breakthrough time could be the cause of this. The second highest recovery due to surfactant flooding was for sample FD3H (2.04 %). This sample had 8.45 cc of residual oil left within the core after waterflooding. After surfactant flooding, an additional 0.17 cc was expelled out of the rock. And finally, the core with the lowest recovery, (0.56 %), was sample FD4H. This sample had 6.17 cc of residual oil left within the core after waterflooding. After surfactant flooding, an additional 0.03 cc was expelled out of the rock.

Despite the fact that the values discussed above seem very trivial, it must be noted that these results are only laboratory scaled. When these results are up-scaled to reservoir context, a recovery of even 0.5 % could lead to a tremendous increase in production and capital.

Detailed calculations of how these values were derived from the measured weights, using material balance, are discussed above in Chapter III

5.1.7 Summary of Results for Case 1

Table 17 below summarizes the breakthrough times, the maximum pressure drop reached and the ultimate recovery achieved for each flooding test, for each core sample.

Table 17. Summary of Breakthrough Time, Maximum Pressure & Ultimate Recovery - Case 1

	Breakthrough Times			Maximum ΔP			Ultimate Recovery		
	Min.			*Psi*			*(% of OOIP)*		
	FD3H	FD4H	FD5C	FD3H	FD4H	FD5C	FD3H	FD4H	FD5C
Decane Flooding	7	7.9	29.9	574	793	1529	-	-	-
Waterflooding	9.2	14.7	38.1	837	953	3502	28.78	33.8	37.58
Surfactant Flooding	42.8	61.4	118.9	987	1079	4758	30.23	34.17	40.22

From the summarized table above as well as the detailed results above, results will be summarized with respect to breakthrough time, pressure drop and recovery respectively.

5.1.7.1 Breakthrough Time

With each successive flooding test, the breakthrough time increases for all three core samples. The reason for this increase is due to the successive increase in viscosity with each flooding test ($\mu_{decane} < \mu_{brine} < \mu_{surfactant}$). This is a desirable effect, intended in IOR and EOR, in order to improve the sweep and increase ultimate recovery. This is because, in order to improve the sweep and increase recovery, it is important to reduce the effects of viscous fingering by ensuring that the displacing fluid (brine or surfactant in this case) has a mobility equal to or lower than that of the oil phase. Since mobility is inversely proportional to viscosity, in order to reduce

the mobility it is necessary to increase the viscosity. Therefore, an increase in viscosity of the injectable, for each successive test, results in a decrease in mobility of the displacing fluid. This in turn results in a decrease of viscous fingering and a more piston-like displacement, thus a delay in breakthrough time, and an improvement in sweep.

5.1.7.2 Pressure Drop

With each successive flooding test, the maximum pressure drop (at breakthrough) increases for all three samples. Assuming all other parameters of Darcy's Law are kept constant for a given core, the change in pressure drop is mainly attributed to the change in viscosity. With each successive test, the average viscosity (at breakthrough) increases due to the increase in viscosity of the injected fluid ($\mu_{decane} < \mu_{brine} < \mu_{surfactant}$). Since pressure drop is directly proportional to viscosity in Darcy's Law, pressure drop will increase with successive increase in viscosity for each test.

5.1.7.3 Recovery

Finally, a comprehensive summary will be discussed for the recovery results. First, an observation is made regarding the change in recovery as a function of breakthrough time. As the breakthrough time increases for a given flooding experiment, the ultimate recovery improves. This is because of the reduced mobility of the injectable.

Next, the main recovery results for Case 1 will be summarized in five figures.

Figure 19 below displays the recovery factor as a percentage of the oil in place (% OIP) for both primary recovery and secondary recovery.

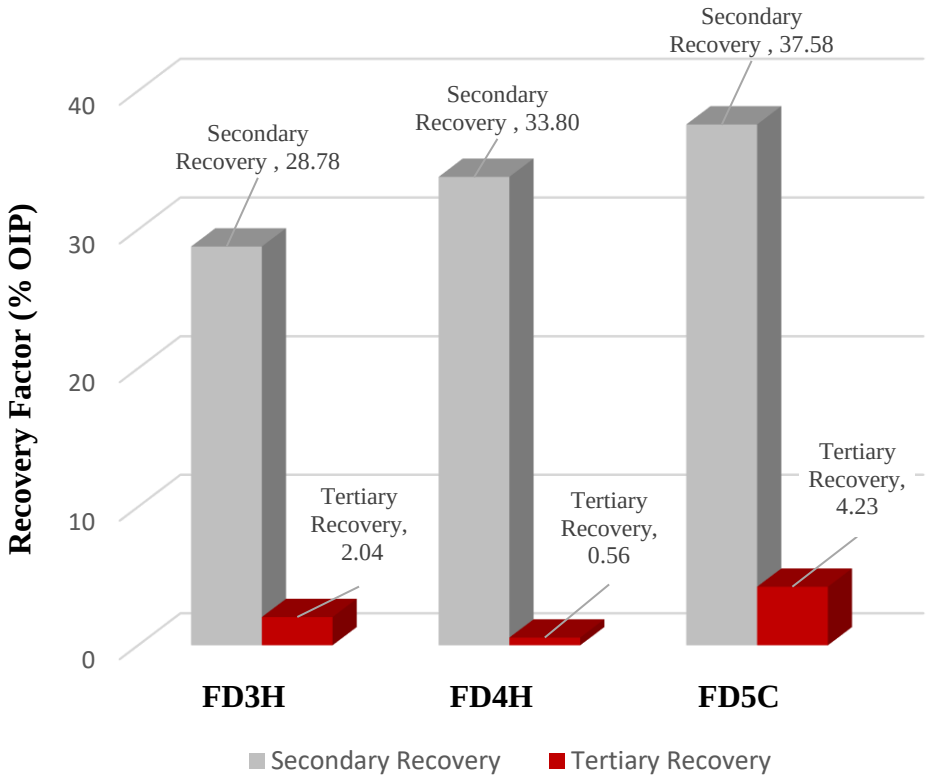

Figure 19. Recovery Factor for both Recovery Methods (% OIP) - Case 1

The recovery due to secondary recovery waterflooding (% of OIP) is 28.78 %, 33.80 %, and 37. 58 % for FD3H, FD4H, and FD5C respectively. The recovery due to tertiary recovery surfactant flooding (% of OIP) is 2.04 %, 0.56 % and 4.23% for FD3H, FD4H, and FD5C respectively. FD5C has the highest recovery for both secondary recovery and for tertiary recovery.

Figure 20 below displays the recovery factor as a percentage of the original oil in place (% OOIP) for both primary recovery and secondary recovery.

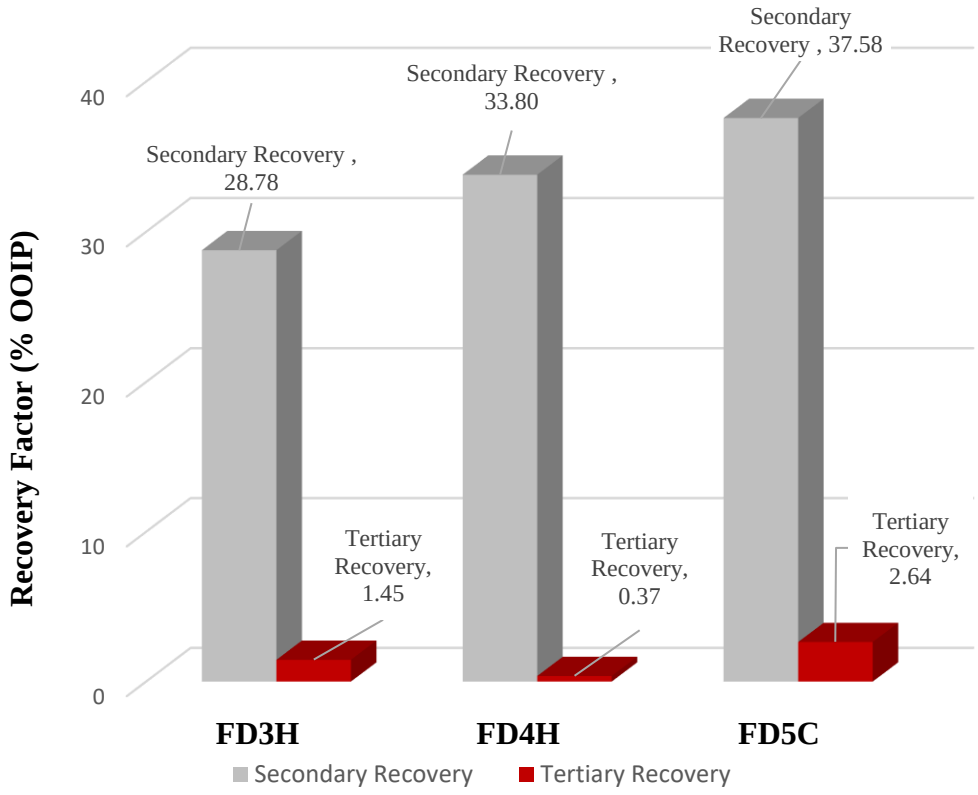

Figure 20 Recovery Factor for both Recovery Methods (% OOIP) - Case 1

The recovery due to secondary recovery waterflooding (% OOIP) is still 28.78 %, 33.80 % and 37. 58 % for FD3H, FD4H, and FD5C respectively. The recovery due to tertiary recovery surfactant flooding place (% OOIP) is 1.45 %, 0.37 % and 2.64% for FD3H, FD4H, and FD5C respectively. Again, FD5C has the highest recovery for both secondary recovery and for tertiary recovery.

Figure 21 below displays the ultimate recovery factor as a percentage of the original oil in place (% OOIP). That is, the total recovery attained through both primary and secondary recovery.

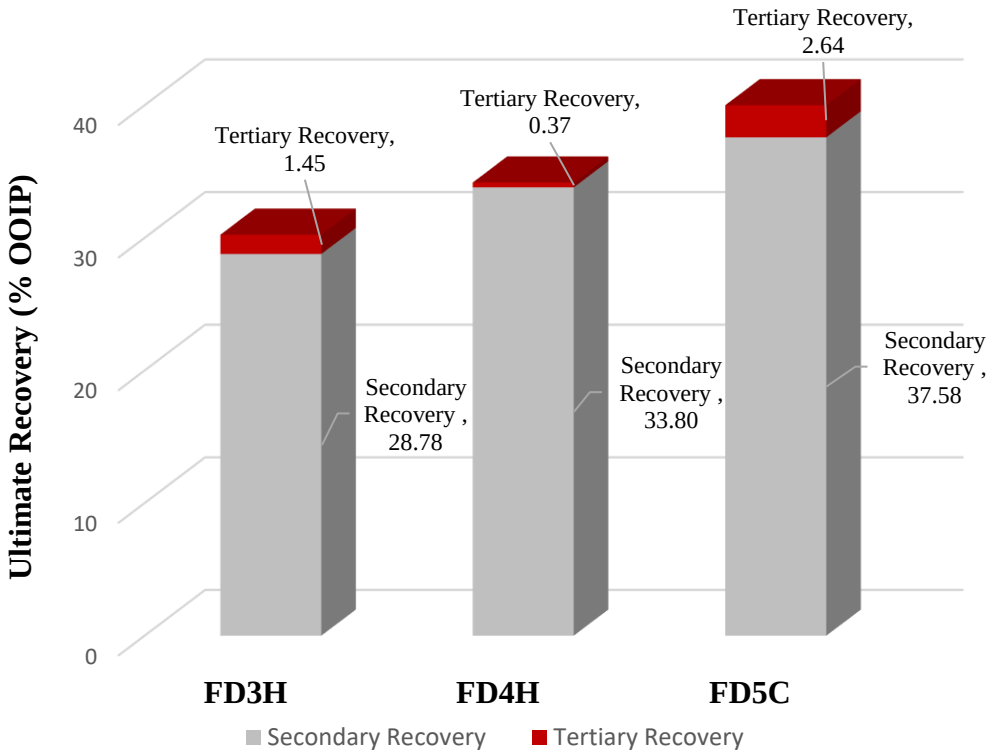

Figure 21. Ultimate Recovery (% of OOIP) - Case 1

The ultimate recovery for sample FD3H is 30.23 %, the ultimate recovery for sample FD4H is 34.17 % and the ultimate recovery for sample FD5C is 40.22%.

Figure 22 below displays the oil in place after the consecutive recovery techniques.

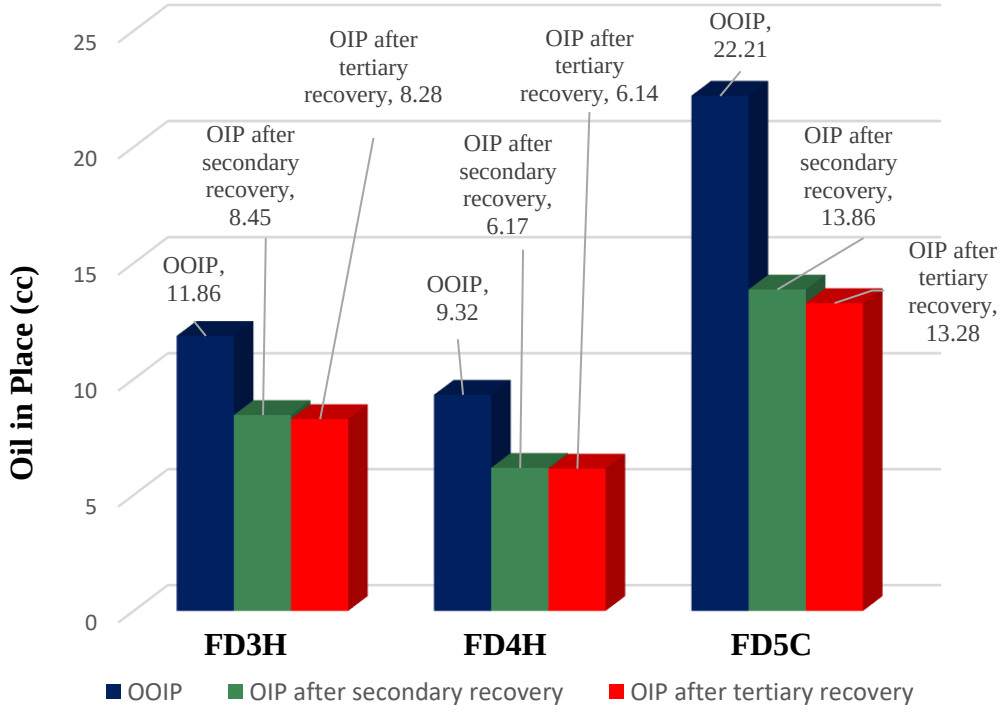

Figure 22. Oil in Place after Consecutive Recovery Techniques - Case 1

The figure above shows how the oil in place reduces after each consecutive recovery technique. For example, of 11. 86 cc of oil initially inside sample FD3H, the volume of oil was reduced to 8.45 cc after waterflooding and then to 8.28 cc after surfactant flooding. It is impossible to achieve 100% recovery but is important to implement tertiary recovery EOR in order to minimize the residual oil saturation.

5.2 Case 2: Fractured Carbonate Samples

For Case 2 the results will be described in the same order as Case 1. Please note that although the cores were not fractured from the very start of the experimental procedure (to ensure proper brine and decane saturation) the results will be discussed in a manner that assumes the cores were fractured from the start. Thus, the order of the results for this section will not necessarily reflect the order of the experimental procedure. For example, the dry *fractured* weight, for each core, was obtained at the end of all experiments, after the core was washed and dried, however, the results obtained from it, such as porosity, will be discussed at the start of the results.

5.2.1 Core Parameters

Table 18 below presents the initial core parameters for two fractured carbonate samples. The parameters include length, diameter, cross sectional area, bulk volume and dry mass. Please note that dry weight measurement refers to the dry fractured weight of the core which includes the rock foil jacketing and the fracture filling.

Table 18. Core Parameters - Case 2

Core Sample	Length	Diameter	Cross Section Area	Bulk Volume	Dry Mass
	L	D	A_{cs}	V_{bulk}	m_{dry}
	cm	*Cm*	cm^2	*Cc*	*g*
FD3H	12.93	3.76	11.10	143.53	321.289
FD4H	13.09	3.76	11.10	145.36	322.72

From **Table 18**, it can be observed that the samples have the same dimensions as before. Essentially, the same rock samples are being used but with a fracture this time. The fracture thickness was adjusted such that the initial core diameter was preserved. The only difference worth noting is that the dry mass decreased in comparison to Case 1 due to the rock material that was lost during the fracture creation.

5.2.2 Porosity

The porosity was only derived through Archimedes' method of weights in Case 2. **Table 19** below summarizes the porosity and pore volume results for the two core samples.

Table 19. Porosity Values obtained from Archimedes' Method - Case 2

Core Sample	Fractured Brine Saturated Mass	Volume of Pores	Bulk Volume	Porosity
	$m_{f\ brine\ saturated}$	V_{pore}	V_{bulk}	Φ
	g	*cc*	*cc*	*%*
FD3H	321.29	24.50	143.53	17
FD4H	322.72	25.00	145.36	17

From **Table 18**, it can be concluded that porosity calculations for Case 2 show that FD3H and FD4H still have almost identical porosities (17 %) and pore volumes (25 cc) as was observed in Case 1. As expected, introducing a fracture in Case 2 caused the porosity and pore volume to increase compared to the values obtained in Case 1.

5.2.3 Oil Flooding

Similar to Case 1, the first of the flooding procedures to take place was decane oil flooding. Oil flooding was done pre-fracturing to ensure proper decane saturation, so the results displayed below will be very similar to the decane flooding results of Case 1. Again, the details of this process and the calculations are described in earlier sections. A real time plot of the pressure drop across the core vs. the elapsed time was plotted for the two samples. **Figure 23** below shows a plot of the pressure drop vs. elapsed time for FD3H and FD4H, and **Figure 24** depicts the same but as function of the number of injected pore volumes.

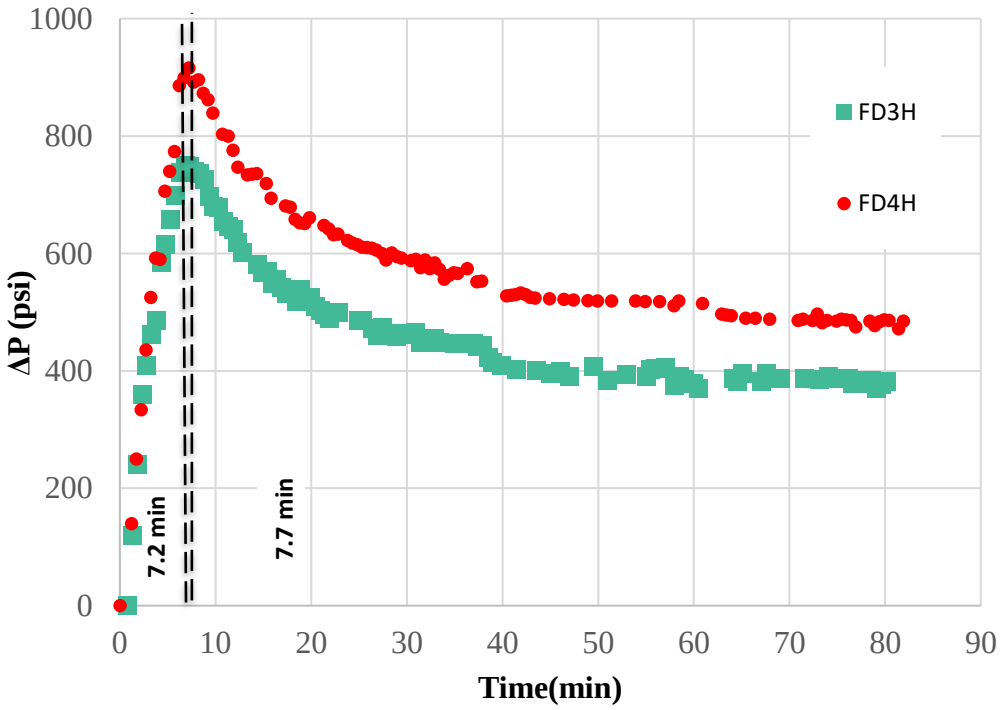

Figure 23. Decane Flooding - ΔP (psi) vs. Time (min) - Case 2

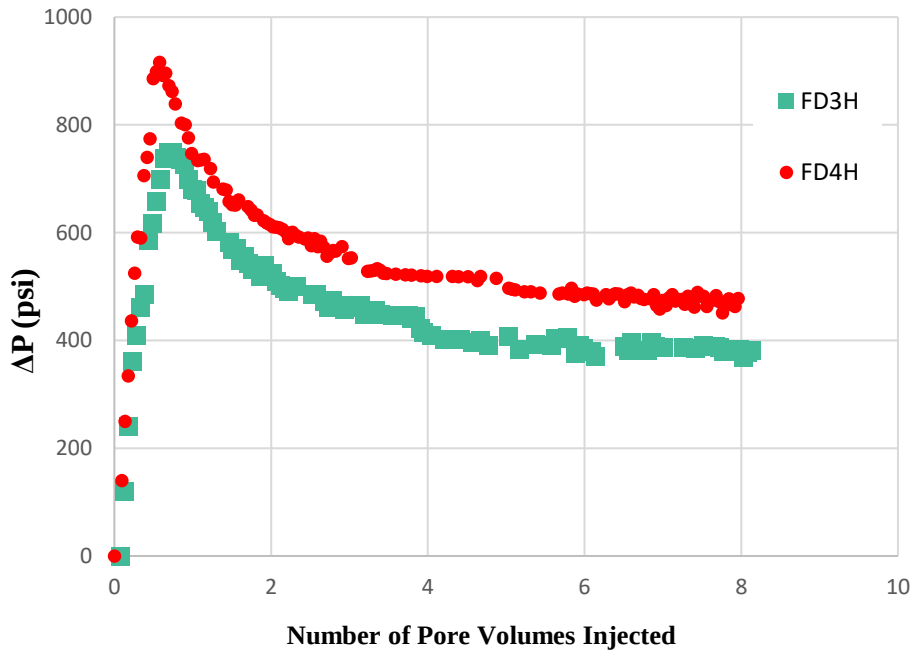

Figure 24. Decane Flooding - ΔP (psi) vs. Number of Injected Pore Volumes - Case 2

From both **Figure 23** and **Figure 24** we can see that the general trend is very similar to the trends observed in **Figure 13** and **Figure 14** in Case 1. Since no fracture has been introduced yet, the above results are a replica of the decane flooding results observed in Case 1 for samples FD3H and sample FD4H. The pressure ranges differ slightly due to experimental uncertainties.

Table 20 below summarizes the breakthrough times for both core samples. These breakthrough times are again almost identical to the ones observed in Case 1.

Table 20. Breakthrough Times of Fractured Samples following Decane Flooding - Case 2

Core Samples	Breakthrough Time *min*
FD3H	7.2
FD4H	7.7

Table 21 below summarizes the core properties after decane flooding was complete and the samples were weighed.

Table 21. Fractured Core Properties following Oil Flooding - Case 2

Core Sample	Fractured Brine/ Decane Saturated Mass $m_{f\ (brine + oil)\ saturated}$	Volume of Oil V_{oil}	Volume of Brine V_{brine}	Oil Saturation S_o	Residual Water Saturation S_{wr}
	g	*cc*	*cc*		
FD3H	340	21.65	2.85	0.88	0.12
FD4H	344.00	14.56	10.44	0.58	0.42

Table 21 above shows the fractured mass after decane flooding ($\mathbf{m_{f\ (brine + oil)\ saturated}}$), the volume of decane oil within the rock ($\mathbf{V_{oil}}$), the volume of brine within the rock ($\mathbf{V_{brine}}$), the initial oil saturation ($\mathbf{S_o}$) and the irreducible water saturation ($\mathbf{S_{wr}}$). Again, FD4H had the lowest oil saturation ($S_o = 0.58$), whereas FD3H had a higher oil saturation ($S_o = 0.88$). Detailed calculations of how these values were derived, using material balance, are discussed above in the Theory section (Chapter III). These parameters now describe a core containing both brine and decane, thus representing a fractured core under reservoir conditions.

5.2.4 Waterflooding

The first of the recovery procedures to take place following brine and decane saturation is waterflooding. Again, the details of this process and the calculations are described in earlier sections. A real time plot of the pressure drop across the core vs. elapsed time was plotted for both samples. Similarly, the same was done as a function of injected pore volumes. **Figure 25** below shows a plot of the pressure drop vs. elapsed time for FD3H and FD4H, and **Figure 26** depicts the same but as function of the number of injected pore volumes.

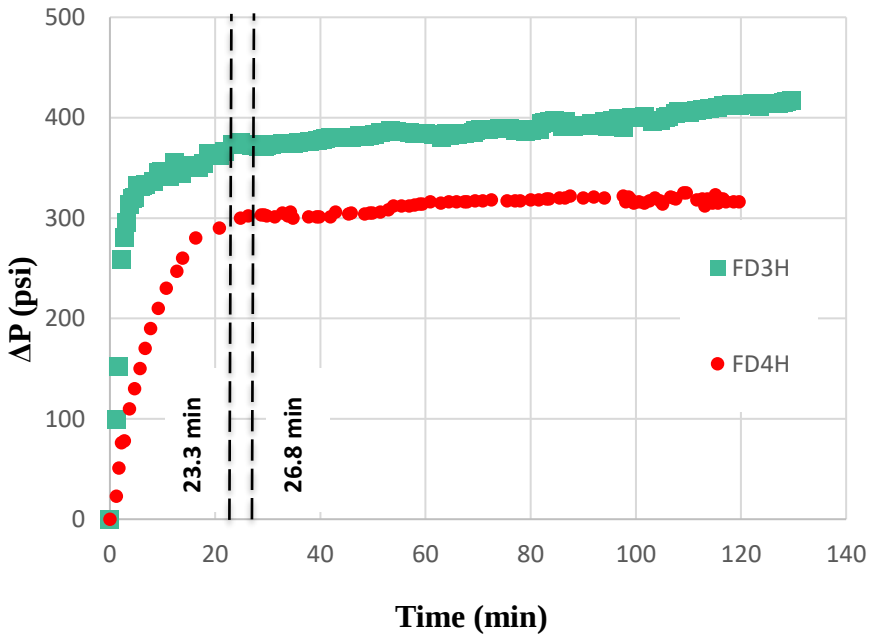

Figure 25. Waterflooding - ΔP (psi) vs. Time (min) - Case 2

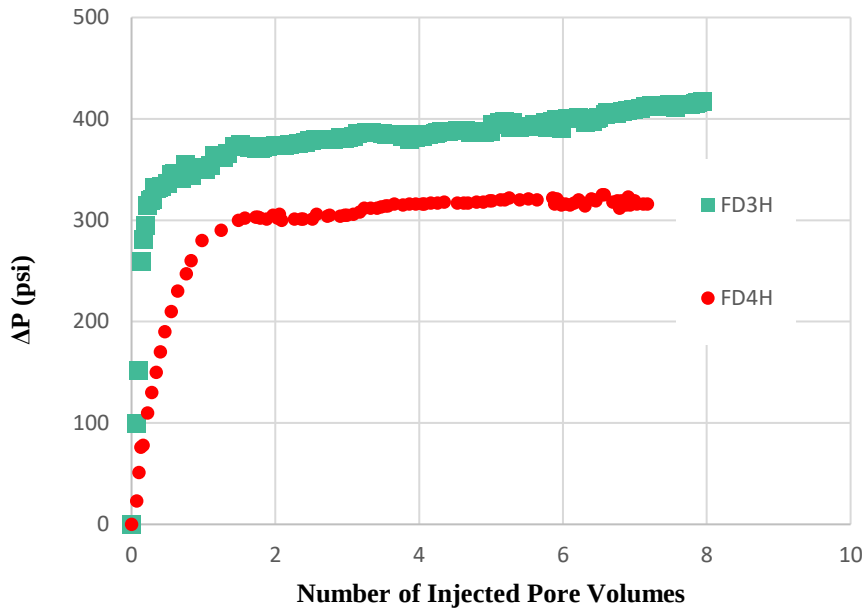

Figure 26. Waterflooding - ΔP (psi) vs. Number of Injected Pore Volumes - Case 2

From both **Figure 25** and **Figure 26** we can see that there is a sharp increase in the pressure drop prior to breakthrough and then a steady incline (almost plateau) after breakthrough is reached. As brine is injected, the pressure increases due to compressibility effect. However this time, the pressure will not increase as much as it did for waterflooding in Case 1 since the core now has a high permeability channel (fracture). The pressure will continue to increase due to the greater rate of fluid inflow into the core compared to fluid outflow out of the core. Once breakthrough point is reached, this is the point at which the first drop of brine is observed to leave the core. Compression effects become less significant and viscosity effects take over. Again, viscous fingering is not as severe here as it was in decane flooding (explained in Case 1 waterflooding), thus at breakthrough it is expected that the vast majority of decane is displaced and that the average

viscosity remains almost constant. Hence, by Darcy's law the pressure drop is expected to reach a steady state. But since the pressure does not reach a complete steady state and remains to increase gradually, it is suspected that there was an early breakthrough through the fracture and other portions of the core were not swept yet.

Since no permeability tests were done for the cores in Case 2, the relationship between the breakthrough time and permeability is not discussed. However, from the graph above we can see that this time, FD3H has a longer breakthrough time (28.8 min) in comparison to FD4H (23.3 min). Therefore, we can predict that the permeability of FD4H is slightly higher than FD3H after the fracture. **Table 22** below summarizes the breakthrough times for the two core samples.

Table 22. Breakthrough Times of Fractured Core Samples following Waterflooding - Case 2

Core Samples	Breakthrough Time *min*
FD3H	26.8
FD4H	23.3

Table 23 below summarizes the core properties after waterflooding was complete and the samples were weighed.

Table 23. Fractured Core Properties following Waterflooding - Case 2

Core Sample	Fractured Core Mass after Waterflooding $m_{f\ waterflooding}$	Volume of Oil V_{oil}	Volume of Brine V_{brine}	Residual Oil Saturation S_{or}	Water Saturation S_w	Volume of Oil expelled ΔV_{oil}	Recovery R
	g	*cc*	*cc*			*cc*	*%*
FD3H	341.31	17.13	7.37	0.70	0.30	4.52	20.86
FD4H	345.12	10.70	14.30	0.43	0.57	3.86	26.50

Table 23 above shows the fractured core mass after waterflooding (**$m_{f\ waterflooding}$**), the volume of oil within the rock (**V_{oil}**), the volume of brine within the rock (**V_{brine}**), the residual oil saturation (**S_{or}**), the water saturation (**S_w**), the volume of oil expelled due to waterflooding (**ΔV_{oil}**) and the percentage recovery obtained from waterflooding (**R**).

From **Table 23**, it can be concluded that secondary recovery was somewhat efficient, but not as efficient as in Case 1. The recovery due to waterflooding was in the range of 20 - 26 %. FD4H had a recovery of 26.6 % and FD3H had a recovery of 20.86 %. In case 1, FD4H had a waterflooding recovery of 33.8 %. After introducing the fracture, the same core had a lower waterflooding recovery of 26.6%. Similarly, FD3H had a recovery of 28.78 % in Case 1. After introducing the fracture, the same core had a lower waterflooding recovery of 20.86 %. For FD4H, the recovery due to waterflooding decreased by 7.2 %, and for FD3H, the recovery decreased by 7.92 %. The results prove that waterflooding is an inefficient recovery technique in carbonate reservoirs, especially in the presence of a fracture. The reason for this is primarily due to water's tendency to flow through the high channel, leaving large portions unswept.

Detailed calculations of how these values were derived using mass material balance are discussed above in the theory section (Chapter III).

5.2.5 Foam Flooding

Following secondary recovery, enhanced oil recovery (foam flooding) was implemented. Again, the details of this process and the calculations are described in earlier sections. The general term ‘foam flooding’ will be used to describe a sequence of two injections:

1. A short foam injection
2. A longer brine injection

A live plot of pressure drop vs. elapsed time (**Figure 27**) was plotted for foam flooding for sample FD3H. The same was plotted as a function of injected pore volumes of foam (**Figure 28**). These live plots display data for foam injection only and not for the brine injection which follows the foam. Results were only obtained for sample FD3H due to a failed quality check for sample FD4H. It is predicted that a malfunction may have occurred in the sensors of the apparatus during FD4H testing.

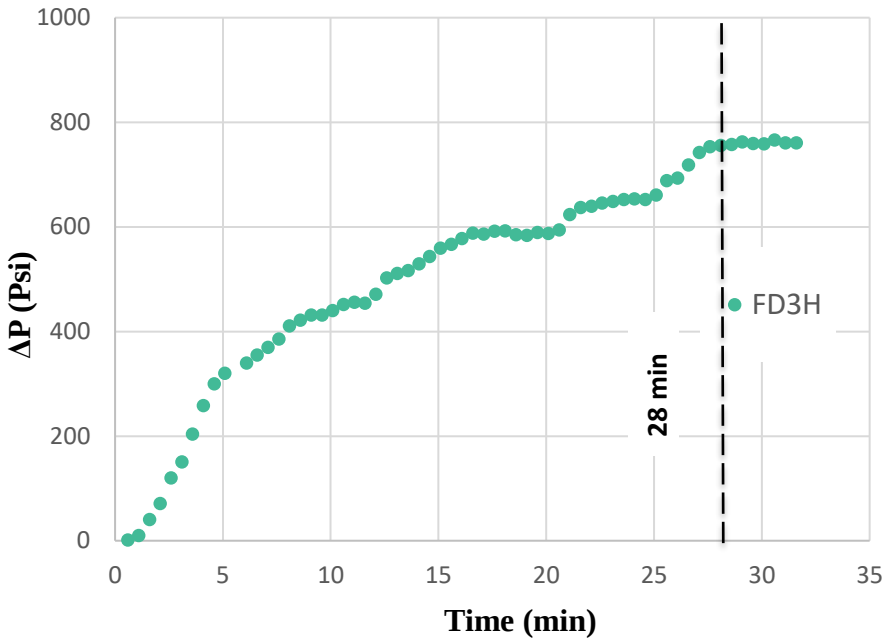

Figure 27. Foam flooding - ΔP (Psi) vs. Time (min) - Case 2

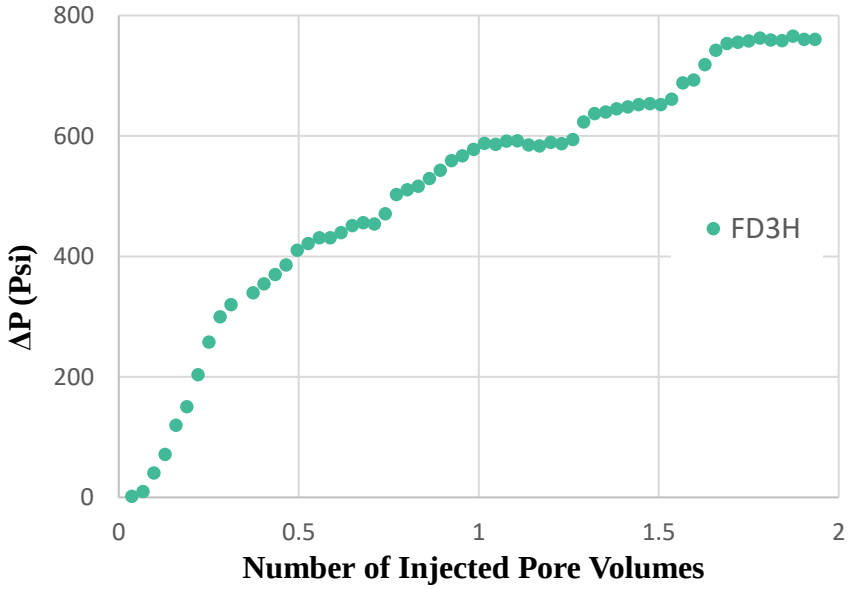

Figure 28. Foam flooding - ΔP (Psi) vs. Number of Injected Pore Volumes - Case 2

From both **Figure 27** and **Figure 28** we can see that there is a sharp increase in the pressure drop at the start. As foam is injected, the pressure increases due to compressibility effect. The maximum pressure drop is relatively low as the core is fractured. The pressure will continue to increase due to the greater rate of fluid inflow into the core compared to fluid outflow out of the core. However, the general pressure trend is not as uniform as earlier tests and exhibits a 'step-like' increase. This could possibly be due to non-uniform sweep by foam (a two-phase mixture), and/or the fractured nature of the core. The core eventually reaches breakthrough at around 28 minutes. The test was stopped, but the pressure was expected to remain somewhat steady.

Table 24 below summarizes the core properties after foam flooding (foam followed by water injection) was complete and the samples were weighed.

Table 24 . Core Properties Following Foam Flooding - Case 2

Core Sample	Fractured Core Mass after Foam flooding	Volume of Oil	Volume of Brine	Residual Oil Saturation	Water Saturation	Volume of Oil expelled	Recovery	
	$m_{f\ foam\ flooding}$	V_{oil}	V_{brine}	S_{or}	S_w	ΔV_{oil}	R	R
	g	*cc*	*cc*			*cc*	*%*	*% of OOIP*
FD3H	341.67	15.89	8.61	0.65	0.35	1.24	7.24	5.73
FD4H	345.3	10.08	14.92	0.4	0.6	0.62	5.83	4.29

The above table shows the mass of the fractured cores after foam flooding ($\mathbf{m_{f\ foam\ flooding}}$). Again, foam flooding refers to the sequential injection of foam followed by brine. The table also displays the volume of oil within the core ($\mathbf{V_{oil}}$), the volume of brine within the core ($\mathbf{V_{brine}}$), the residual oil saturation ($\mathbf{S_{or}}$), the water saturation ($\mathbf{S_w}$), the additional volume of oil expelled due to foam flooding ($\mathbf{\Delta V_{oil}}$), the percentage recovery obtained from foam flooding (**R**), as well as the recovery as a % of the OOIP (**R**).

The volume of foam within the core ($\mathbf{V_{foam}}$) is not included in the table above. This is because it is assumed that the flushing fluid (brine) following foam injection will expel all of the foam out of the rock. Even though it is understood that some residual foam will remain within the core, this assumption was made in order to solve the material balance with two unknowns ($\mathbf{V_{oil}}$ and $\mathbf{V_{brine}}$).

From **Table 24**, it can be concluded that tertiary recovery foam flooding was efficient. The recovery due to foam flooding, as a percentage of OIP (oil in place), was in the range of 5 - 8%. FD3H had a higher foam recovery factor (7.24 % of OIP) compared to FD4H (5.83% of OIP). Of a residual oil volume of 17.13 cc left within the core (FD3H) after waterflooding, an additional 1.24 cc were expelled after foam flooding. And of a residual oil volume of 10.7 cc left within the core (FD4H) after waterflooding, an additional 0.62 cc were expelled after foam flooding.

The recovery due to foam flooding, as a percentage of the original oil in place (OOIP), is in the range of 4 - 6%. Again, FD3H had a higher recovery factor (% of OOIP) due to foam flooding (5.73 %) compared to FD4H (4.29 %). Of an initial oil volume of 21.65 cc within core FD3H, an additional 5.73 % of this volume is extracted due to foam flooding. And of an initial oil volume of 14.56 cc within core FD4H, an additional 4.29 % of this volume is extracted due to foam flooding.

Despite the fact that these recoveries seem somewhat trivial, it must be noted that these results are only laboratory scaled. Once these results are up-scaled to reservoir context, it becomes evident that an additional recovery in the range of 4 - 6 % (% of OOIP) could lead to a tremendous increase in production and capital.

Detailed calculations of how these values were derived using mass material balance are discussed above in the theory section (Chapter III).

5.2.6 Summary of Results for Case 2

Table 25 below summarizes the breakthrough times, the maximum pressure drop reached and the ultimate recovery achieved for each flooding test, for each core sample.

Table 25. Summary of Breakthrough Time, Maximum Pressure and Ultimate - Case 2

	Breakthrough Times		Maximum ΔP		Ultimate Recovery	
	min		Psi		(% of OOIP)	
	FD3H	FD4H	FD3H	FD4H	FD3H	FD4H
Decane Flooding	7.2	7.7	916	740	_	_
Waterflooding	26.8	23.3	417	316	20.86 %	26.50 %
Foam Flooding	28	NA	760.51	NA	26.6 %	30.79 %.

From the summarized table above as well as the detailed results above, results will be summarized with respect to breakthrough time, pressure drop and recovery respectively.

5.1.6.1 Breakthrough Time

With each successive flooding test, the breakthrough time increases. The reason for this increase is due to the successive increase in viscosity with each flooding test ($\mu_{decane} < \mu_{brine} < \mu$

$_{foam}$). As discussed in Case 1, an increase in viscosity of the injectable, for each successive test, results in a decrease in mobility of the displacing fluid. This in turn results in a decrease of viscous fingering and a more piston-like displacement, thus a delay in breakthrough time, and an improvement in sweep.

5.1.6.2 Pressure Drop

With each successive flooding test, the maximum pressure drop increases for both samples. The maximum pressure does not necessarily occur at breakthrough in this case. Assuming all other parameters of Darcy's Law are kept constant for a given core, the change in pressure drop is mainly attributed to the change in viscosity. With each successive test, the average viscosity increases. Since pressure drop is directly proportional to viscosity in Darcy's Law, pressure drop will increase with successive increase in viscosity for each test.

5.1.6.3 Recovery

Finally, a comprehensive summary will be discussed for the recovery results. First, an observation is made regarding the change in recovery as a function of breakthrough time. As the breakthrough time increases for a given flooding experiment, the ultimate recovery improves. This is because of the reduced mobility of the injectable.

Next, the main recovery results for Case 2 will be summarized in five figures. **Figure 29** below displays the recovery factor as a percentage of the oil in place (% OIP) for both primary recovery and secondary recovery.

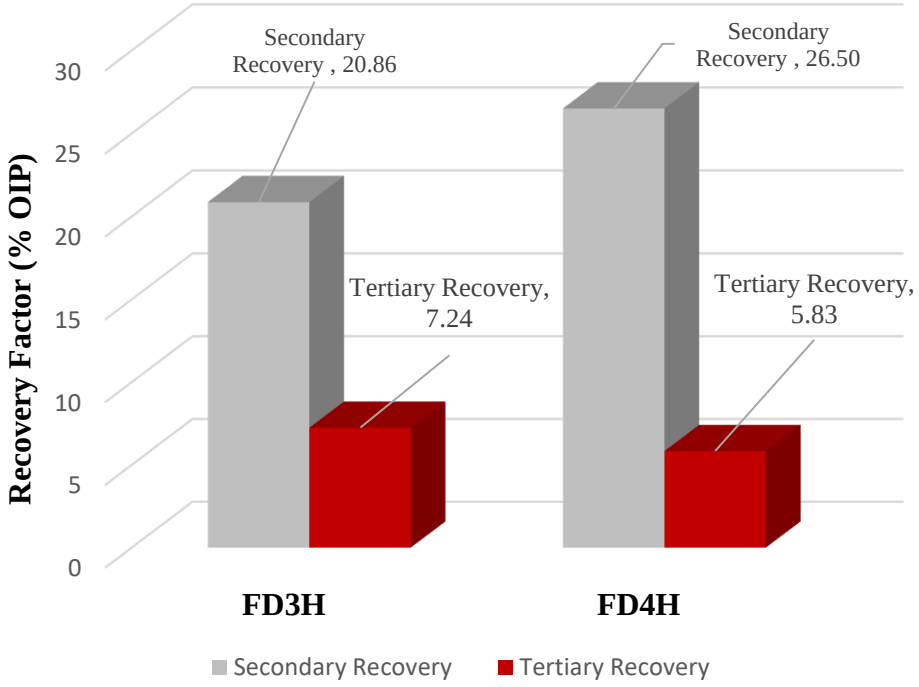

Figure 29. Recovery Factor for both Recovery Methods (% OIP) - Case 2

The recoveries due to secondary recovery waterflooding (% of OIP) are 20.86 % and 26.50 % for FD3H and FD4H respectively. The recoveries due to tertiary recovery foam flooding (% of OIP) are 7.24 % and 5.83 % for FD3H and FD4H respectively.

Figure 30 below displays the recovery factor as a percentage of the original oil in place (OOIP) for both primary recovery and secondary recovery.

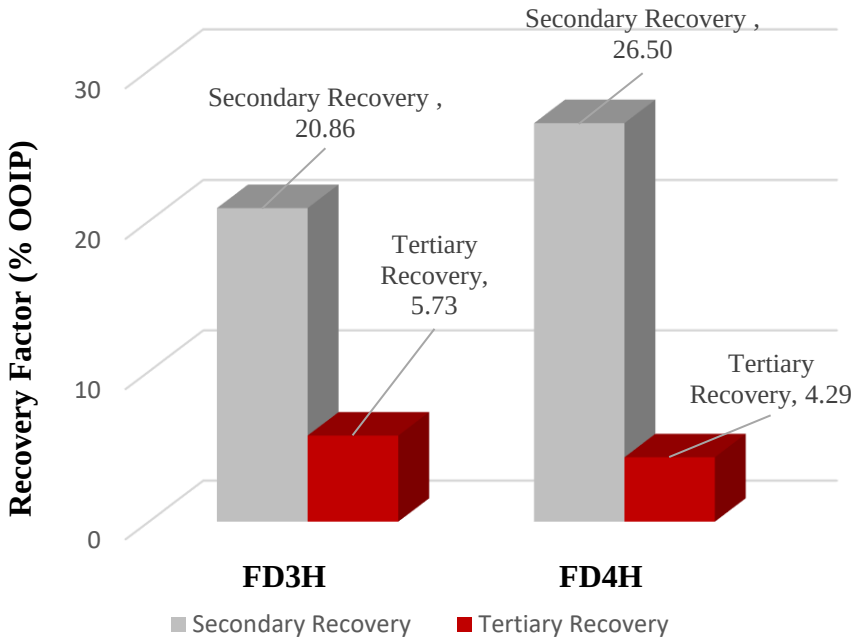

Figure 30. Recovery Factor for both Recovery Methods (% OOIP) - Case 2

Secondary recovery due to waterflooding (% OOIP) is still 20.86 % and 26.50 % for FD3H and FD4H respectively. Tertiary recovery due to foam flooding (% of OOIP) is 5.73 % and 4.29 % for FD3H and FD4H respectively.

Figure 31 below displays the ultimate recovery factor as a percentage of the original oil in place (% OOIP). That is, the total recovery attained through both primary and secondary recovery.

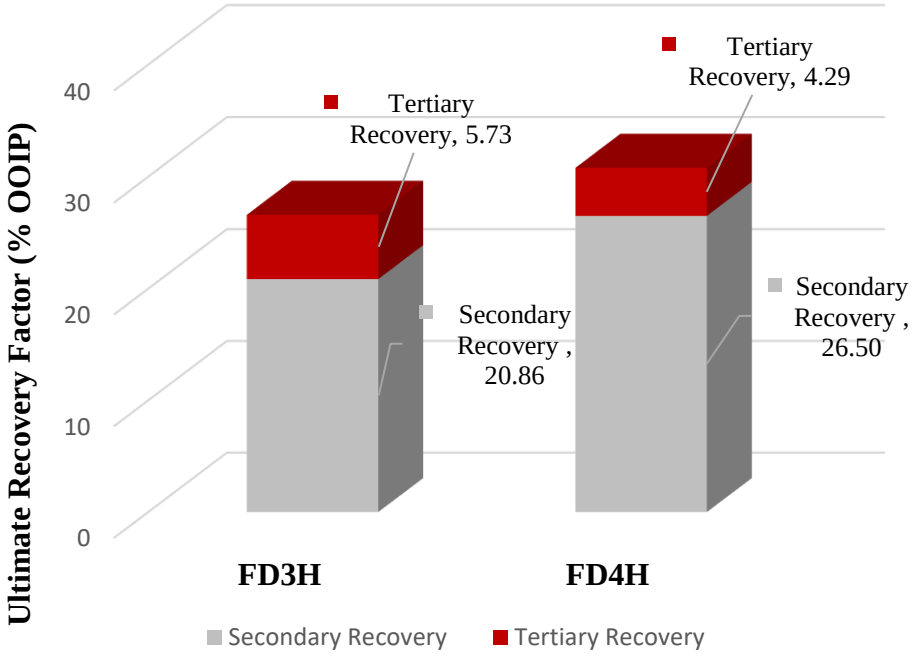

Figure 31. Ultimate Recovery Factor (% OOIP) - Case 2

The ultimate recovery for sample FD3H is 26.6 % and the ultimate recovery for sample FD4H is 30.79 %.

Figure 32 below displays the oil in place after the consecutive recovery techniques.

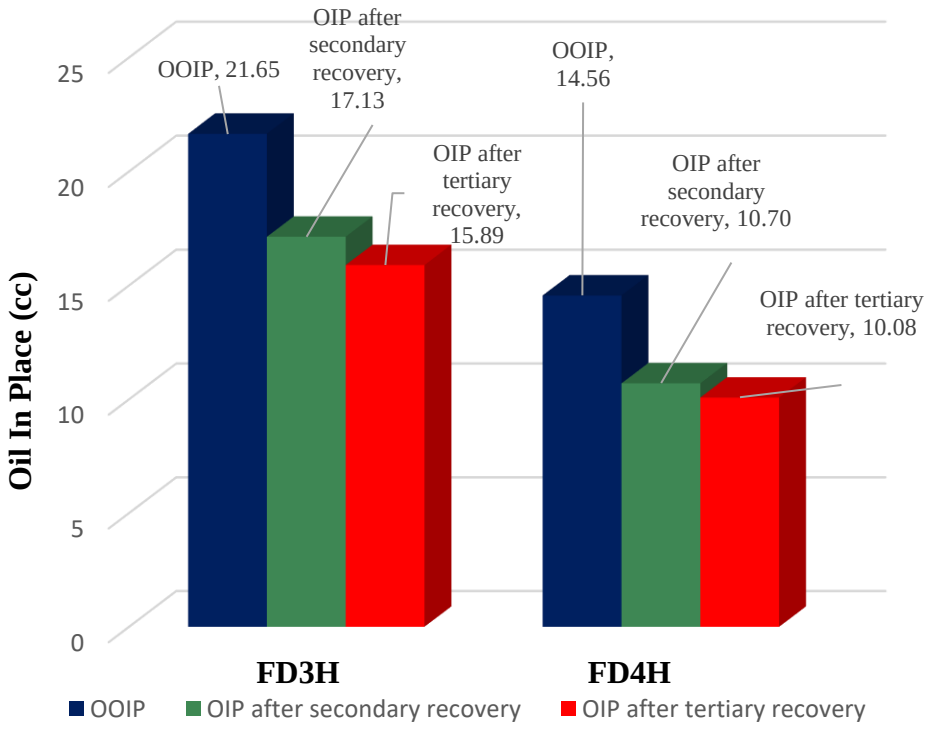

Figure 32. Oil in Place after Consecutive Recovery Techniques - Case 2

The figure above shows how the oil in place reduces after each consecutive recovery technique. For example, of 21.65 cc of oil initially present inside sample FD3H, the volume of oil was reduced to 17.13 cc after waterflooding, and then to 15.89 cc after foam flooding. It is impossible to achieve 100% recovery but is important to implement tertiary recovery in order to minimize the irreducible oil saturation.

5.3 Summary and Comparison of Cases

5.3.1 Summary

In Case 1, a sequence of experiments were carried out to investigate secondary recovery (waterflooding) and tertiary recovery (surfactant flooding), in three non-fractured carbonate samples.

In Case 2, a sequence of similar experiments were carried out to investigate secondary recovery (waterflooding) and tertiary recovery (foam flooding), in two fractured carbonate samples. The two cores used in this case were previously used in Case 1.

In Case 1, the overall recovery (as a % of the OOIP) obtained was 30.23 %, 34.17 % and 40.22 % for samples FD3H, FD4H and FD5C, respectively. Most of the recovery was due to waterflooding, and a small fraction due to surfactant flooding. The enhancement in recovery due to surfactant flooding was in the range of 0.5 to 4.5 % (as a % of the OOIP). For the surfactant concentration used (0.1 vol. %), this recovery is very reasonable. Literature provides slightly higher recoveries using surfactant of much higher concentrations (2-8 %) [13]. However, in industry enhanced oil recovery comes with a cost and high concentration surfactants may not be cost effective. A 0.1 vol. % concentration of surfactant is much cheaper and will offer a considerable increase in recovery when up-scaled.

In Case 2, the overall recovery (as a % of the OOIP) obtained was 26.6 % and 30.79 % for samples FD3H, and FD4H respectively. Naturally, the majority of oil recovered was due to waterflooding, with a smaller fraction due to foam flooding. The enhancement in recovery due to foam flooding was in the range of 4 to 6 % (as a % of the OOIP). Again, foam was composed of the same surfactant concentration (0.1 %) and nitrogen. Therefore, the results obtained for the concentrations selected prove to be very good.

5.3.2 Comparison between Both Cases

While in both cases waterflooding accounted for the majority of the recovery achieved, the recovery due to waterflooding in Case 1 is considerably higher than the recovery due to waterflooding in Case 2. Proving the central issue this thesis seeks to solve: secondary recovery performs poorly in fractured carbonates (Case 2). This is because brine passes through the high permeability fracture channel leaving significant portions unswept. While the recovery due to waterflooding for Case 2 was less than for Case 1, the overall recovery of Case 2 increased when foam was introduced. Due to the properties of foam discussed in the introduction and its ability to partially plug the fracture, the post-foam flushing fluid (brine) was able to sweep some more of the residual oil left behind. After foam flooding, the overall recovery as a % of the OOIP increased significantly to approach the value of overall recovery as a % of the OOIP achieved in Case 1. However, it did not exceed it. This is due to the inherent properties of fractured formations when compared to a non-fractured formations.

CHAPTER VI

CONCLUSION

In summary, the demand for crude oil is continuous. Carbonate reservoirs constitute of over half of the world's oil reserves. Therefore, the issues faced with pre-existing recovery techniques in carbonate reservoirs deserves greater attention.

This thesis has demonstrated two cases to represent two different types of carbonate reservoirs and the applicable EOR technique for each. In Case 1, surfactant flooding was applied to a non-fractured carbonate sample, and in Case 2, foam flooding was applied to a fractured carbonate sample.

In case 1, a 0.1 vol. % surfactant solution was used for EOR. This low concentration was selected to depict an affordable option that can be implemented on large scale production. The enhancement in recovery was in the range of 0.5 to 4.5 % (as a % of the OOIP). For the low concentration used, this recovery provides good results. The surfactant increased the recovery by decreasing the oil-water interfacial tension as well as changing the rock wettability from oil-wet towards water-wet, making it easier to extract the oil.

In Case 2, foam was used for EOR. Foam was composed of nitrogen and surfactant of the same concentration (0.1 vol. %). A low concentration was used for the same reasons. The enhancement in recovery due to foam flooding was in the range of 4 to 6 % (as a % of the OOIP). For the low concentration of surfactant used, this recovery provides very good results. Foam increased the recovery due to two reasons: one, improving the sweep efficiency, and two, improving the displacement efficiency. The sweep efficiency is mainly improved by plugging the high permeability fracture and thus forcing the post-foam flooding fluid (brine) to sweep the lower

permeability areas of the core, and the displacement efficiency is improved due to the decrease in oil-water interfacial tension.

While waterflooding was effective in both cases, it was less effective in Case 2. This proves the limitation of pre-existing secondary recovery techniques in fractured carbonate reservoirs. When foam was injected the overall recovery increased significantly, approaching the overall recovery achieved in Case 1.

Understanding the optimum balance between surfactant concentration, cost and profitability would be recommended for the future. It may also be worthwhile to investigate other types of surfactants for EOR.

REFERENCES

1. Arhuoma, M.; Yang, D. Y.; Dong, M. Z.; Li, H.; Idem, R. Numerical simulation of displacement mechanisms for enhancing heavy oil recovery during alkaline flooding. Energy Fuels. 23 (2009) 5995-6002.

2. Casteel, J. F.; Djabbarah, N. F. Sweep improvement in CO2 flooding by use of foaming agents. SPE reservoir engineering 3 (1988) 1186-1192.

3. N. Quennouz, M. Ryba, J.-F. Argillier, B. Herzhaft, Y. Peysson and N. Pannacci*. Microfluidic Study of Foams Flow for Enhanced Oil Recovery (EOR). Oil Gas Sci. Technol. – Rev. IFP Energies nouvelles, 69 (2014) 457-466.

4. Pei, H. H.; Zhang, G. C.; Ge, J. J.; Tang, M. G.; Zheng, Y. F. Comparative effectiveness of alkaline flooding and alkaline–surfactant flooding for improved heavy-oil recovery. Energy Fuels. 26 (2012) 2911-2919.

5. Seethepalli, A.; Adibhatla, B; Mohanty, K. K. Physicochemical interactions during surfactant flooding of fractured carbonate reservoirs. SPE journal 9 (2004) 411-418.

6. Sun, Q.; Li, Z. M.; Li, S. Y.; Jiang, L.; Wang, J. Q.; Wang, P. Utilization of surfactant-stabilized foam for enhanced oil recovery by adding nanoparticles. Energy Fuels 28 (2014) 2384-2394.

7. Sun, Q.; Li, Z.; Jiqian, W.;Li, S. Aqueous foam stabilized by partially hydrophobic nanoparticles in the presence of surfactant. Colloids and Surfaces A: Physicochemical and Engineering Aspects, 471 (2015) 54-64.

8. Xie, W. Y.; Li, X. G.; Chen, Z. Y. Review of exploration and development technologies for heavy oil and high pour-point oil in Liaohe oil region. Acta Pet. Sin. 28 (2007) 145-150.

9. Xin, Y. C.; Dong, X. Y.; Bian, J. P. Affecting factors for flow ability of high-salinity heavy oil and methods for improving oil mobility. Acta Pet. Sin. 31 (2010) 480-485.

10. Yao, C. J.; Lei, G. L.;, Li, L.; Gao, X. M. Selectivity of pore-scale elastic microspheres as a novel profile control and oil displacement agent. Energy Fuels 26 (2012) 5092-5101.

11. Zerhboub, M.; Touboul, E.; Ben-Naceur, K.; Thomas, R. L. Matrix acidizing: a novel approach to foam diversion. SPE Production & Facilities 9 (1994), 121-126.

12. Zuta, J.; Fjelde, I.; Berenblyum, R.; Leif, H. V.; Ovesen, H. Modeling of transport of a CO_2-foaming agent during CO_2-foam processes in a fractured chalk rock. Proceedings of the SPE Improved Oil Recovery Symposium; Tulsa, Oklahoma, USA, April 24-28, 2010; SPE paper 129601.

13. Ahmadi, Mohammad Ali, and Seyed Reza Shadizadeh. “Implementation of a High-Performance Surfactant for Enhanced Oil Recovery from Carbonate Reservoirs.” Journal of Petroleum Science and Engineering.,110 (2013) 66–73.

14. Llave, F. M.; Chung, F. T-H.; Louvier, R. W.; Hudgins, D. A. Foams as mobility control agents for oil recovery by gas displacement. *Proceedings of the SPE/DOE Enhanced Oil Recovery Symposium*; Tulsa, Oklahoma, April 22-25, **1990**; SPE paper 20245.